ACS APPLIED MATERIALS & INTERFACES

Research Article

www.acsami.org

Two Analogous Polyhedron-Based MOFs with High Density of Lewis Basic Sites and Open Metal Sites: Significant CO_2 Capture and Gas Selectivity Performance

Bing Liu,[†] Shuo Yao,[†] Xinyao Liu,[†] Xu Li,[‡] Rajamani Krishna,[§] Guanghua Li,[†] Qisheng Huo,[†] and Yunling Liu*[,†]

[†]State Key Laboratory of Inorganic Synthesis and Preparative Chemistry, College of Chemistry, Jilin University, Changchun 130012, PR China

[‡]Department of Chemical and Bimolecular Engineering, National University of Singapore, 117576 Singapore

[§]Van 't Hoff Institute for Molecular Sciences, University of Amsterdam, Science Park 904, 1098 XH Amsterdam, The Netherlands

Supporting Information

ABSTRACT: By means of modulating the axial ligand and adopting supermolecular building blocks (SBBs) strategy, two polyhedron-based metal−organic frameworks (PMOFs) have been successfully synthesized $[Cu_6(C_{17}O_9N_2H_8)_3(C_6H_{12}N_2)(H_2O)_2(DMF)_2]\cdot 3DMF\cdot 8H_2O$ (**JLU-Liu46**) and $[Cu_6(C_{17}O_9N_2H_8)_3(C_4H_4N_2)(H_2O)_2(DMF)_2]\cdot 3DMF\cdot 8H_2O$ (**JLU-Liu47**), which possess a high density of Lewis basic sites (LBSs) and open metal sites (OMSs). Since the size of axial ligand in **JLU-Liu47** is smaller than that in **JLU-Liu46**, **JLU-Liu47** shows larger pore volume and higher BET surface area. Then, the adsorption ability of **JLU-Liu47** for some small gases is better than **JLU-Liu46**. It is worthwhile to mention that both of the two compounds exhibit outstanding adsorption capability for CO_2 ascribed to the introducing of urea groups. In addition, the theoretical ideal adsorbed solution theory (IAST) calculation and transient breakthrough simulation indicate that **JLU-Liu46** and **JLU-Liu47** should be potential materials for gas storage and separation, particularly for CO_2/N_2, CO_2/CH_4, and C_3H_8/CH_4 separation.

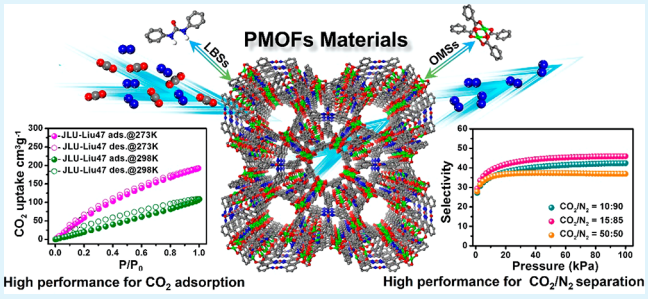

KEYWORDS: *polyhedron metal−organic frameworks, MOP cages, porous materials, CO_2 capture, gas separation*

INTRODUCTION

The sharp increasing of CO_2 in the atmosphere, produced by the burning of fossil fuels (such as coal, oil, and natural gas), has led to global warming.[1−5] Therefore, reducing the CO_2 emissions and developing clear energy sources have become the most urgent environmental issues. Currently, promoting the CO_2 capture and separation technologies will play a fatal role in dealing with the problems.

Metal−organic frameworks (MOFs), which have significant applications in gas capture, storage, and separation, are a new kind of promising advanced materials compared to the traditional porous zeolites and carbon materials.[6−13] Besides, metal−organic polyhedral (MOP) which owns a large-void cage and open-channel type is a prominent building unit to construct MOFs with large pore volume, high surface area, and excellent gas uptake capacity.[14−17] For the sake of constructing polyhedron-based metal−organic frameworks (PMOFs), a supermolecular building blocks (SBBs) approach is considered an effective strategy which has been used to configure a series of classic PMOFs, such as *rht*-MOFs,[18] *gea*-MOFs,[19] and *fcu*-MOFs.[20] In addition, it also indicates that the ligands, with functional groups such as amino, imino, amide, urea, imidazole, and triazole in the PMOFs may significantly improve the storage and separation performance for CO_2. Therefore, many PMOFs modified with functional groups have been reported, such as NU-100,[21] Cu-TPBTM,[22] PCN-6x series,[23] Cu-TDPAT,[24] Cu-TATAB,[25] HUNST-5,[26] and so forth. As for PCN-61 and Cu-TPBTM, although the pore size, surface area, and the number of open metal sites (OMSs) for the two MOFs are almost same, the CO_2 adsorption performance is different because the functional group is −C≡C− in PCN-61 and −NH−CO− in Cu-TPBTM.

In terms of isophthalate moiety making it convenient to construct MOP cage, the tetracarboxylic acid ligand with two isophthalate moieties is a commendable candidate to synthesize PMOFs. However, most tetracarboxylic ligands are conditioned to assemble *nbo* topology without MOP cages, such as MOF-505,[27] MOF-101,[28] UTSA-80,[29] PCN-16,[30] NOTT-105,[31] and NU-135.[32] In our preliminary work, a ligand with both tetracarboxylic and triazole moieties has been selected to

Received: July 25, 2017
Accepted: September 7, 2017
Published: September 7, 2017

DOI: 10.1021/acsami.7b10795
ACS Appl. Mater. Interfaces 2017, 9, 32820−32828

successfully construct two novel PMOFs materials, **JLU-Liu20** and **JLU-Liu21**, which display significant capture capacity of CO_2.[33] In order to improve the properties of CO_2 adsorption and separation, urea groups which possesses a high density of Lewis basic sites (LBSs) have been introduced as functional group to replace the triazole moieties in the tetracarboxylic ligand and a less used ligand 5,5′-(carbonylbis(azanediyl))-diisophthalic acid (**H_4L**) is successfully prepared. Up to now, only two MOFs (NU-601[34] and $Eu_4[L]_3$[35]) based on H_4L ligand have been reported, and neither of them possess MOP cage nor adsorption abilities. Opportunely, we have successfully prepared a PMOF $[Cu_6(C_{17}O_9N_2H_8)_3(C_6H_{12}N_2)(H_2O)_2(DMF)_2]\cdot 3DMF\cdot 8H_2O$ (**JLU-Liu46**) which is made up of three different kinds of MOP cages and possesses a high density of OMSs and LBSs. In consideration of the 1,4-diazabicyclo[2.2.2]-octane (DABCO) in the framework occupies a certain amount of space, and a similar but smaller pyrazine ligand is adopted to construct the same framework. Just as we expected, another analogous PMOF $[Cu_6(C_{17}O_9N_2H_8)_3(C_4H_4N_2)(H_2O)_2(DMF)_2]\cdot 3DMF\cdot 8H_2O$ (**JLU-Liu47**) with larger pore volume than **JLU-Liu46** is successfully synthesized. Both of the compounds exhibit excellent properties in small gases adsorption (CO_2, CH_4, C_2H_6, and C_3H_8), especially for CO_2. Meanwhile, the simulation method of ideal adsorbed solution theory, breakthrough, and Grand Canonical Monte Carlo Simulations are applied to evaluate the gas selective separation abilities. The simulation results indicate that both **JLU-Liu46** and **JLU-Liu47** are promising materials for gas capture and separation.

EXPERIMENTAL SECTION

Materials and Methods. Ligand **H_4L** was synthesized in accordance with the literature procedure.[34] The structural characterization is shown in Scheme S1 and Figure S1. ^{1}H NMR (300 MHz, DMSO-d_6, δ, ppm) 13.24 (s, 4H), 9.64 (d, 2H), 8.34 (d, J = 1.5 Hz, 4H), 8.12 (d, J = 3 Hz, 2H).

All chemicals were purchased from chemical company and used without additional purification. Powder X-ray diffraction (PXRD) pattern were recorded on a Rigaku D/max-2550 diffractometer with Cu Kα radiation (λ = 1.5418 Å). Elemental analyses (C, H, and N) were performed on a vario MICRO elementary analyzer. The thermal gravimetric analyses (TGA) were carried out on a TGA Q500 thermogravimetric analyzer with a heating rate of 10 °C min^{-1} in air.

Synthesis of Compounds. *Synthesis of **JLU-Liu46**.* A mixture of $Cu(BF_4)_2\cdot 6H_2O$ (7.5 mg, 0.012 mmol), **H_4L** (2 mg, 0.005 mmol), 1,4-diazabicyclo[2.2.2]-octane (DABCO) (0.1 mL, 2 g in 10 mL DMF), *N*,*N*-dimethylformamide (DMF) (1 mL), ethanol (0.5 mL), H_2O (0.5 mL), and 0.35 mL of HNO_3 (2.7 M in DMF) were put into a 20 mL vial; then, the vial was transferred to an oven and heated at 85 °C for 12 h. Blue crystals were gathered, washed with DMF, and air-dried (58% yield based on $Cu(BF_4)_2\cdot 6H_2O$). Elemental analysis (%) calculated for **JLU-Liu46** $C_{72}H_{91}Cu_6N_{13}O_{42}$: C, 39.45; H, 4.19; N, 8.31. Found: C, 39.93; H, 4.23; N, 8.41. The experimental and simulated PXRD patterns are identical, revealing that the as-synthesized compound is obtained as the pure phase (Figure S9a).

*Synthesis of **JLU-Liu47**.* A mixture of $Cu(BF_4)_2\cdot 6H_2O$ (7.5 mg, 0.012 mmol), **H_4L** (3 mg, 0.0075 mmol), pyrazine (0.15 mL, 2 g in 10 mL DMF), DMF (1 mL), ethanol (0.75 mL), H_2O (0.75 mL), and 0.45 mL of HNO_3 (2.7 M in DMF) were added to a 20 mL vial; then, the vial was put into an oven and heated at 85 °C for 10 h. Blue crystals were collected, washed with DMF, and air-dried (54% yield based on $Cu(BF_4)_2\cdot 6H_2O$). Elemental analysis (%) calculated for **JLU-Liu47** $C_{70}H_{83}Cu_6N_{13}O_{42}$: C, 38.93; H, 3.87; N, 8.43. Found: C, 38.98; H, 3.91; N, 8.38. The experimental and simulated PXRD patterns are identical, revealing that the as-synthesized products are phase pure (Figure S10a).

Single Crystal X-ray Crystallography. Both the crystallographic data of **JLU-Liu46** and **JLU-Liu47** were recorded on a Bruker Apex II CCD diffractometer using graphite-monochromated Mo Kα (λ = 0.71073 Å) radiation at 20 °C. The structures were solved by direct methods and refined by full-matrix least-squares on F^2 using version 5.1.[36] From the difference Fourier map, all non-hydrogen atoms were definitely found and refined anisotropically. The hydrogen atoms of the ligands were generated theoretically onto the specific atoms and refined isotropically with fixed thermal factors. As the guest molecules were highly disordered and could not be modeled properly, the diffused electron densities resulting from them were removed by the SQUEEZE routine in PLATON and the results were appended in the Supporting Information. The reported refinements are of the guest-free structures using the *.hkp files produced on a SQUEEZE routine operations. The final formula of **JLU-Liu46** and **JLU-Liu47** were derived from crystallographic data combined with elemental and thermogravimetric analysis data. Crystallographic data for **JLU-Liu46** and **JLU-Liu47** (CCDC 1555805 and 1555806) have been deposited with Cambridge Crystallographic Data Centre. Data can be found free of charge upon request at www.ccdc.cam.ac.uk/data_request/cif. Crystal data and structure refinement are summarized in Table S1. The topology analysis for **JLU-Liu46** and **JLU-Liu47** was calculated by using TOPOS 4.0 software.[37]

Gas Adsorption Measurements. The adsorption measurements of N_2, CO_2, CH_4, C_2H_6, and C_3H_8 were carried out on a Micromeritics ASAP 2020. In order to completely get rid of the guest solvent molecules, **JLU-Liu46** and **JLU-Liu47** were soaked in ethanol and replaced with absolute ethanol (12 cycles for 3 days), then activated at 95 °C for 10 h under the vacuum. The nonvolatile solvent molecules have mostly been removed during the activation process as confirmed by the TGA data (Figures S11 and S12).

RESULTS AND DISCUSSION

Single-crystal X-ray diffraction analysis reveals that **JLU-Liu46** crystallizes in the tetragonal crystal system with *P*4/*mnc* space group. The framework is aggregated with typical copper paddlewheels and two types of organic linkers (Figure S2), L^{4-} as major linker, and the DABCO as axial ligand, respectively (Figure 1a). As illustrated in Figure 1b, **JLU-Liu46** has three types of cages with large Connolly surface area.

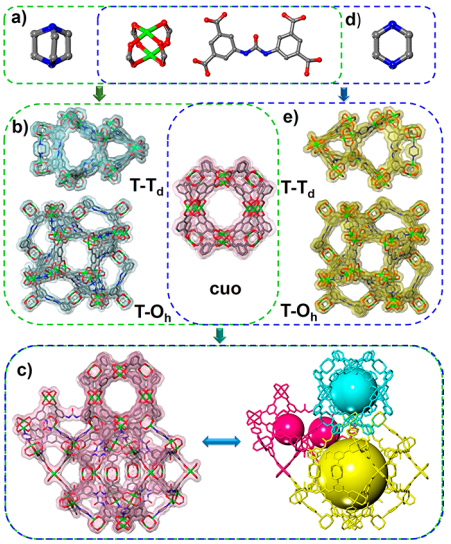

Figure 1. Single-crystal structure for **JLU-Liu46** and **JLU-Liu47**: Cu paddlewheel, organic L^{4-} ligand ,and the axial ligand DABCO (a) and pyrazine (d); three types of cage with Connolly surface areas for **JLU-Liu46** (b) and **JLU-Liu47** (e); (c) arrangement of the three kinds of cage for **JLU-Liu46** and **JLU-Liu47**.

DOI: 10.1021/acsami.7b10795
ACS Appl. Mater. Interfaces 2017, 9, 32820−32828

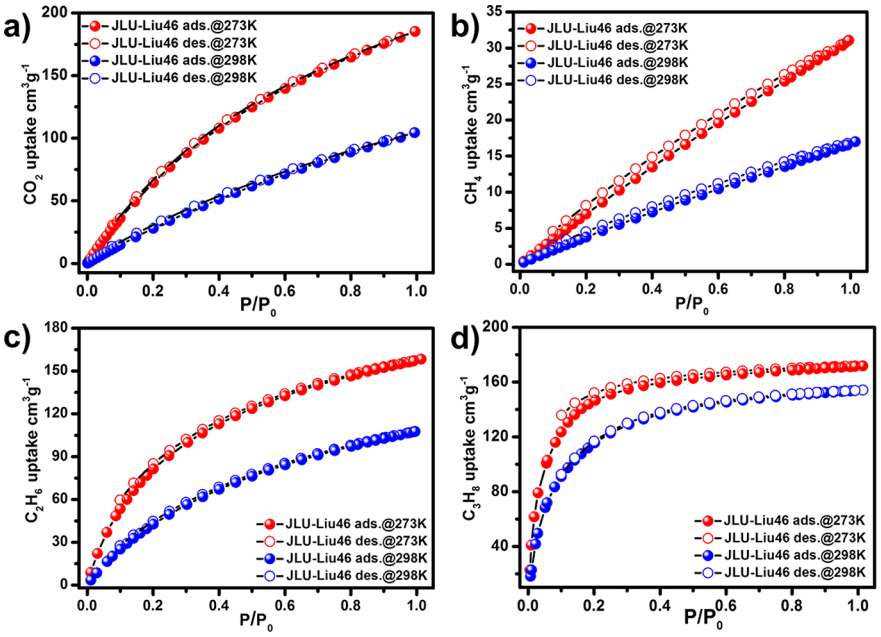

Figure 2. (a) CO_2, (b) CH_4, (c) C_2H_6, and (d) C_3H_8 gas absorption−desorption isotherms for **JLU-Liu46** at 273 and 298 K under 1 atm.

The first kind of cage is the classical MOP-1 with cuboctahedron (*cuo*) geometry ($M_{12}L_{24}$), which consists of 12 copper paddlewheels and 24 L^{4-} ligands. The second kind of cage shows truncated tetrahedron ($T\text{-}T_d$) configuration ($M_{12}L_6$) with 12 copper paddlewheels, 6 L^{4-} ligands, and 4 DABCO ligands. The third cage is the largest one with truncated octahedron geometry ($T\text{-}O_h$) ($M_{24}L_{16}$) which is constructed from 24 copper paddlewheels, 16 L^{4-} and 8 DABCO. The internal diameters of the three kinds of cages are 31 ($T\text{-}O_h$), 12 (*cuo*), and 10 ($T\text{-}T_d$) Å (regardless of the van der Waals radii), respectively (Figures 1c and S5). Then, the assembling of the three different kinds of polyhedron cages leads to the formation of a 3D PMOF. Moreover, **JLU-Liu46** possess multiple pore systems, the diameter of the biggest square channel is approximate to be 6.5 Å × 6.5 Å along the *a* axis (regardless of the van der Waals radii, Figures S3 and S4). Such cages provide a beneficial environment for better access of natural gas and the consequent host−guest interaction. From the view of topology, the Cu-paddlewheels building unit can be simplified as a square, and L^{4-} is seen as a pair of triangle geometries. The overall framework forms a (3, 4)-connected network, and the Schläfli symbol is $\{6^2.8^2.9^2\}^2\{6^2.8\}^4\{6^2.9\}^2\{6^3.8.10^2\}$, which is the same as those of our previously reported **JLU-Liu20** and **JLU-Liu21** materials (Figure S8). The total accessible volume of **JLU-Liu46** calculated by PLATON is 63.0%.

As an axial ligand, DABCO unit connects two adjacent paddlewheels and doubly supports the framework, which greatly enhances the framework rigidity and stability. However, it reduces the size of window for the framework at the same time. In order to mitigate the disadvantage, pyrazine, which has the same shape but smaller size to DABCO, is selected to synthesize another analogous PMOF. Fortunately, the presumptive PMOF **JLU-Liu47** is successfully obtained, which possesses a framework similar to that of **JLU-Liu46** (Figures 1c−e and S6). The structure difference between them is the axial ligand in **JLU-Liu46** is DABCO, while it is pyrazine in **JLU-Liu47**. DABCO, with an axial length of 2.6 Å, is connected to two paddlewheels with a distance of 6.9 Å in **JLU-Liu46**. By contrast, the pyrazine with an axial length of 2.8 Å is linked to two paddlewheels with a distance of 7.1 Å in **JLU-Liu47**. Hence, the windows in **JLU-Liu46** are smaller than those in **JLU-Liu47** (Figure S7). Moreover, the larger transverse dimension of DABCO (4.0 Å) makes **JLU-Liu46** own smaller accessible pore volumes (63.0%) than **JLU-Liu47** (66.5%), which can be verified by PLATON. Therefore, the adsorption performance of **JLU-Liu47** will be changed compared to **JLU-Liu46**.

Thermal Stability Analyses. The thermal stability of **JLU-Liu46** and **JLU-Liu47** are estimated by variable-temperature powder X-ray diffraction (VTPXRD) and thermogravimetric analysis (TGA), cooperatively. In the respect of VTPXRD, both of the compounds can keep its integrity until 200 °C (Figures S9b and 10b). From the TGA point of view, **JLU-Liu46** can be steady to 250 °C, and the 42.9% weight loss is attributed to the release of guest molecules. Subsequently, the framework collapsed and displays 37.2% (calcd 36.8%) weight loss (Figure S11). Similarly, **JLU-Liu47** shows 32.3% weight loss before 250 °C and a further 38.9% (calcd 37.8%) weight loss until 450 °C (Figure S12).

Gas Adsorption of JLU-Liu46 and JLU-Liu47. The reversible type I isotherm obtained by N_2 adsorption measurement at 77 K verify the permanent porosities of **JLU-Liu46** and **JLU-Liu47** (Figure S13). The Brunauer−Emmett−Teller (BET) surface area of **JLU-Liu46** is calculated to be 1787 $m^2\ g^{-1}$, and the Langmuir surface area is 2400 $m^2\ g^{-1}$. The experimental total pore volume resulted from the N_2 isotherm was found to be 0.87 $cm^3\ g^{-1}$, which is pretty close to the theoretical pore volume (0.91 $cm^3\ g^{-1}$). Owing to the multiple pore systems, high density of OMSs/LBSs, and surface areas of **JLU-Liu46**, it also features good adsorption capacity for other small gases.

The CO_2 uptake of **JLU-Liu46** is determined to be 185 (36.3 wt %) and 104 (20.4 wt %) $cm^3\ g^{-1}$ at 273 and 298 K under 1 atm, respectively, much higher than those of most reported MOFs materials, such as Zn-MOF-74 (17.6 wt %),[38] $Cu_3(BTC)_2$ (18.4 wt %),[39] and PCN-6 (15.9 wt %).[40] Due to the high density of LBSs and OMSs which provide a larger

DOI: 10.1021/acsami.7b10795
ACS Appl. Mater. Interfaces 2017, 9, 32820−32828

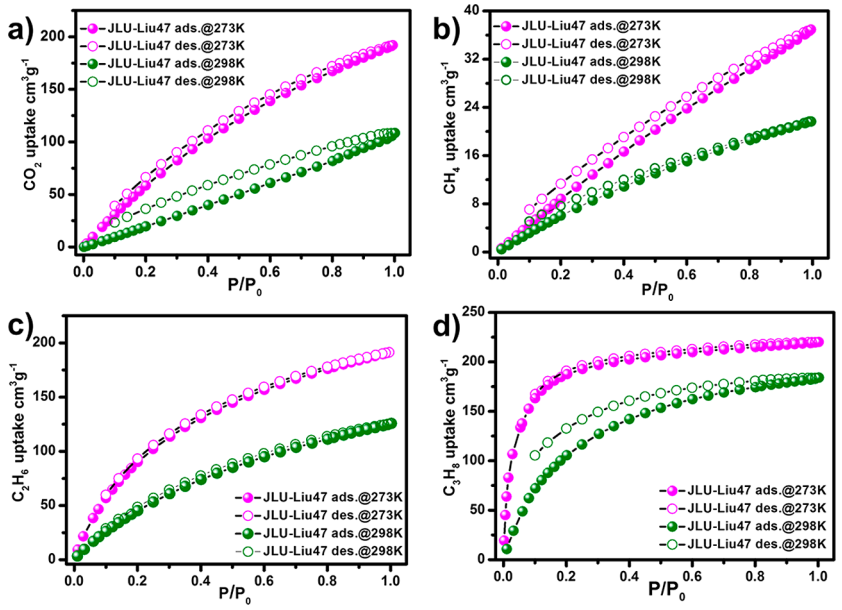

Figure 3. (a) CO_2, (b) CH_4, (c) C_2H_6, and (d) C_3H_8 gas absorption−desorption isotherms for **JLU-Liu47** at 273 and 298 K under 1 atm.

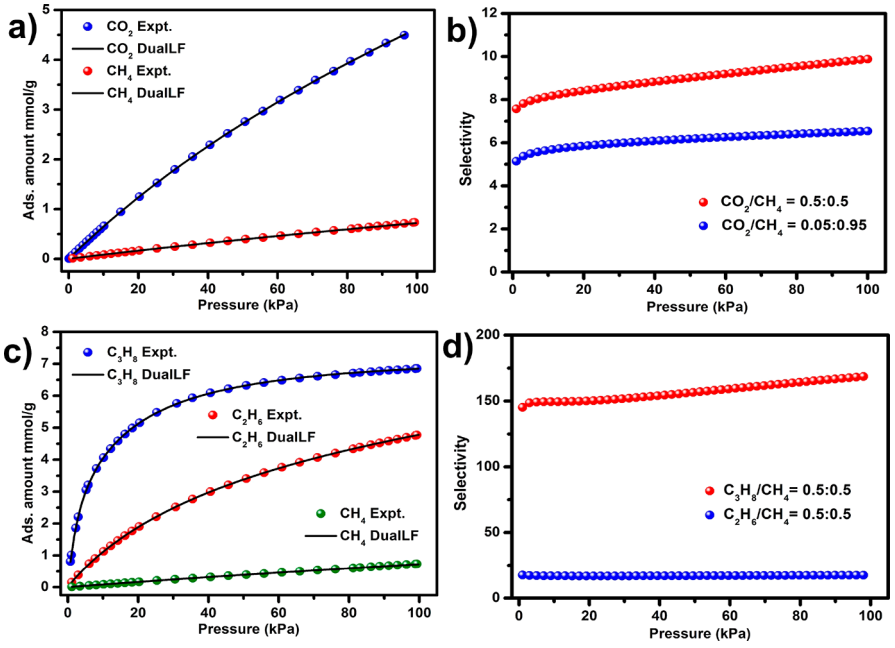

Figure 4. CO_2, CH_4, C_2H_6, and C_3H_8 adsorption isotherms at 298 K along with the dual-site Langmuir Freundlich (DSLF) fits (a, c); Gas mixture adsorption selectivity are predicted by IAST at 298 K and 100 kPa for **JLU-Liu46** (b, d).

number of force sites for CO_2 molecules, **JLU-Liu46** exhibits outstanding adsorption capacity of CO_2. This result suggests that **JLU-Liu46** could be a good candidate for CO_2 capture and storage. At zero loading, the adsorption enthalpy of **JLU-Liu46** is 32 kJ mol^{-1} (Figure S15a), higher than those of the MOFs based on Cu-paddlewheel unit and multidentate carboxylic acid ligand, such as PCN-124 (26.3),[41] PCN-66 (26.2),[23] PCN-61 (22.0),[23] NOTT-125 (25.4),[42] and NOTT-122 (24.5).[43] The adsorption of some other light hydrocarbons CH_4, C_2H_6, and C_3H_8 are also measured at 273 and 298 K under 1 atm, respectively. The maximum uptake for CH_4 is 31 and 17 cm^3 g^{-1}, that for C_2H_6 is 158 and 107 cm^3 g^{-1}, and that for C_3H_8 is 171 and 154 cm^3 g^{-1}, respectively (Figure 2b−d). Furthermore, the Q_{st} of CH_4, C_2H_6, and C_3H_8 are 15, 28, and 33 kJ mol^{-1}, respectively (Figure S15b−d).

As far as **JLU-Liu47**, its BET surface areas and Langmuir surface area were calculated to be 1800 and 2493 m^2 g^{-1}, respectively (Table S2). Rationally, the CO_2, CH_4, C_2H_6, and C_3H_8 adsorption performance for **JLU-Liu47** is better than **JLU-Liu46**. At 273 and 298 K, the maximum adsorption of CO_2 is 192 (37.7 wt %) and 108 (21.2 wt %) cm^3 g^{-1} (Figure 3a). Moreover, the CO_2 adsorption capacity of **JLU-Liu47** increases to 4.3 wt %, and that of **JLU-Liu46** is 2.9 wt % at 298 K and 0.15 bar, which is pointedly higher than many reported Cu-MOFs under the same condition (Table S5). Significantly, in comparison with triazole functionalized MOF **JLU-Liu20**, **JLU-Liu47** shows higher CO_2 uptake at 1 bar (Table S3, S4).

DOI: 10.1021/acsami.7b10795
ACS Appl. Mater. Interfaces 2017, 9, 32820−32828

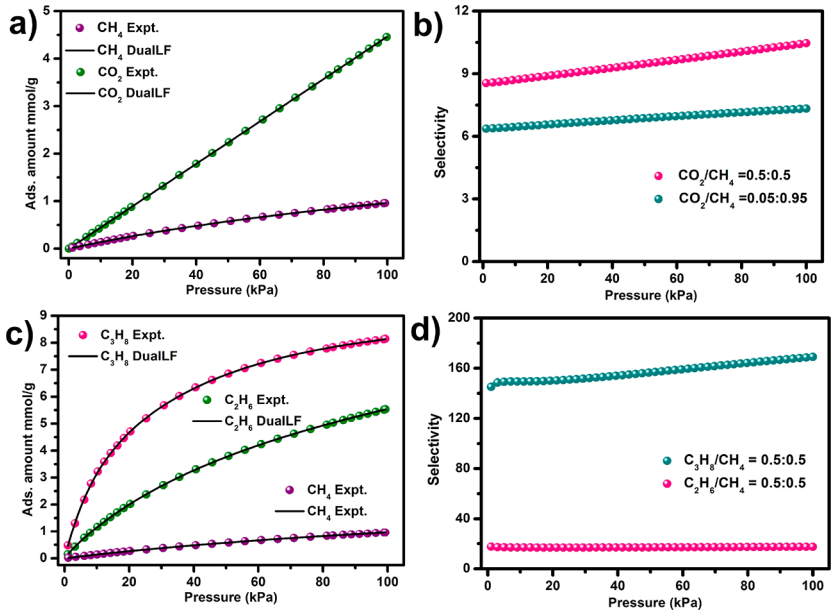

Figure 5. CO_2, CH_4, C_2H_6, and C_3H_8 adsorption isotherms at 298 K along with the dual-site Langmuir Freundlich (DSLF) fits (a, c); gas mixture adsorption selectivity are predicted by IAST at 298 K and 100 kPa for **JLU-Liu47** (b, d).

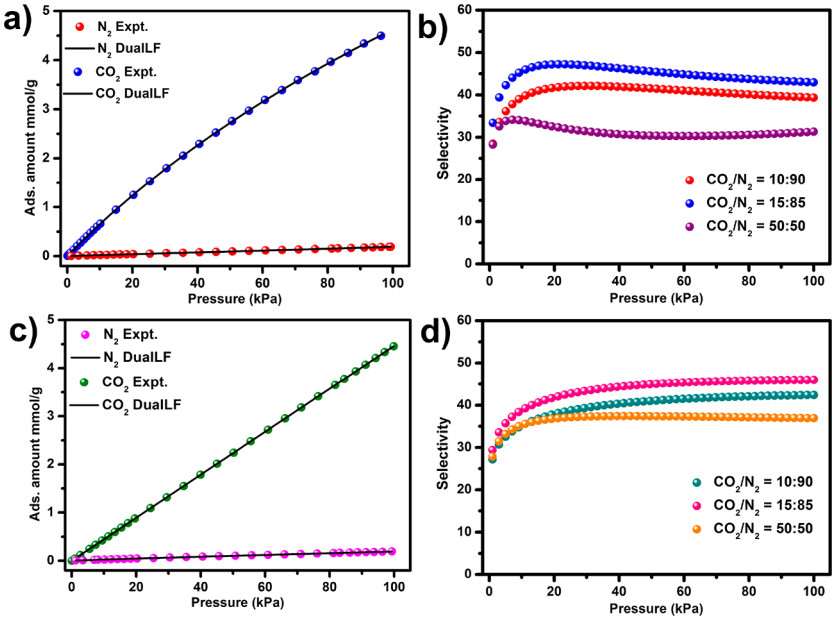

Figure 6. CO_2 and N_2 adsorption isotherms at 298 K along with the dual-site Langmuir Freundlich (DSLF) fits for **JLU-Liu46** (a) and **JLU-Liu47** (c); gas mixture adsorption selectivity are predicted by IAST at 298 K and 100 kPa for **JLU-Liu46** (b) and **JLU-Liu47** (d).

The phenomenon is due to the size of pyrazine is smaller than DABCO, and **JLU-Liu47** has a larger pore volume than **JLU-Liu46**. It is notable that the enthalpy of CO_2 for **JLU-Liu47** reaches up to 35 kJ mol^{-1} (Figure S16a), which is due to the high OMSs density, anionic skeletons, multiple pore systems, and higher surface area of **JLU-Liu47** frameworks coordinately provide stronger interactions to the CO_2 molecules.

Similarly, **JLU-Liu47** has better adsorption capacity for small gas molecules than does **JLU-Liu46**. The maximum adsorption of CH_4 is 36 and 21 cm^3 g^{-1}, that of C_2H_6 is 191 and 125 cm^3 g^{-1}, and that of C_3H_8 is 217 and 182 cm^3 g^{-1}, respectively (Figure 3b–d). Furthermore, the Q_{st} of CH_4, C_2H_6 and C_3H_8 is 16, 28, and 34 kJ mol^{-1}, respectively (Figure S16b–d).

Separation Behaviors of JLU-Liu46 and JLU-Liu47. For the purpose of industrial applications, the selective separation behavior of **JLU-Liu46** and **JLU-Liu47** for CO_2/CH_4, C_2H_6/CH_4, and C_3H_8/CH_4 were calculated by IAST. Subsequently, the fitting parameters are used for the prediction of multicomponent adsorption by IAST. The selectivity of CO_2/CH_4 (50 and 50%; 5 and 95%) is 9.8 and 6.5 for **JLU-Liu46** at 298 K and 1 atm (Figure 4a,b), which are comparable to ZIF-8[44] and some carbon materials[45] under the same conditions. The selectivity of C_2H_6 over CH_4 (50 and 50%) and that of C_3H_8 over CH_4 (50 and 50%) are 17 and 169 at 298 K and 1 atm, respectively (Figure 4c,d).

Besides, with respect to **JLU-Liu47**, the selectivity of CO_2 over CH_4 (50 and 50%; 5 and 95%) is 10.4 and 7.3 (Figure

DOI: 10.1021/acsami.7b10795
ACS Appl. Mater. Interfaces 2017, 9, 32820–32828

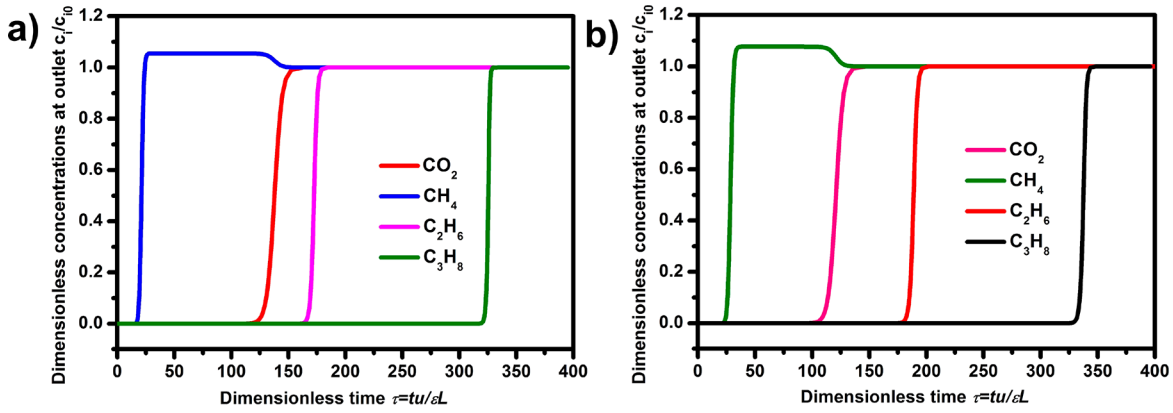

Figure 7. Simulations of transient breakthrough characteristics for equimolar 4-component $CO_2/CH_4/C_2H_6/C_3H_8$ mixture in **JLU-Liu46** (a) and **JLU-Liu47** (b) at 100 kPa and 298 K.

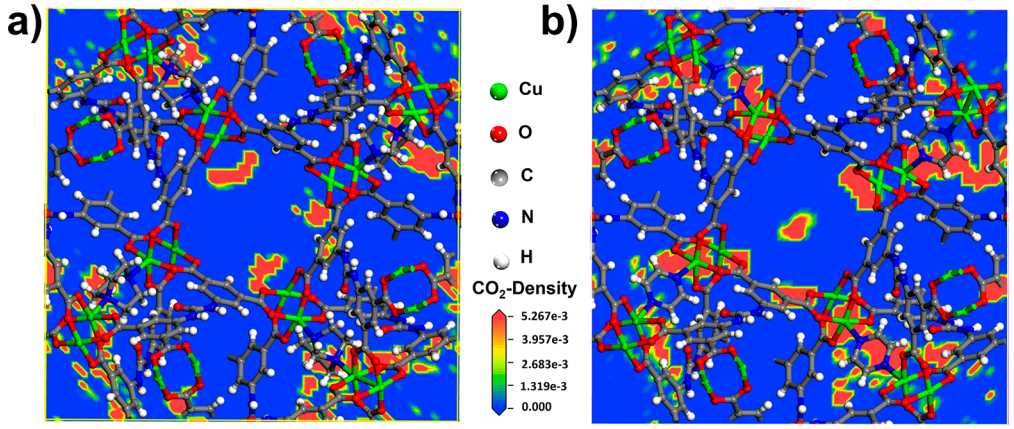

Figure 8. Density distribution of CO_2 molecules center-of-mass of **JLU-Liu46** (a) and **JLU-Liu47** (b) at 298 K and 1 bar simulated by GCMC simulation.

5a,b). As shown in Figure 5, the selectivities for equimolar binary mixtures of C_2H_6 and CH_4 and of C_3H_8 and CH_4 are 17 and 168 (Figure 5c,d), respectively, similar to **JLU-Liu46**. The selectivities of C_3H_8 over CH_4 for **JLU-Liu46** and **JLU-Liu47** are comparable to those of some reported MOFs including LIFM-26 (50),[46] FJI-C1 (78.7),[47] UTSA-35a (80),[48] FIR-7aht (80),[49] eea-MOF-4 (136),[50] and eea-MOF-5 (156).[50] Considering the difference of polarizability and quadrupole moment between CO_2 and CH_4, the significant separation for CH_4 of **JLU-Liu46** and **JLU-Liu47** can be mainly attributed to their multiple cage features, in which the high density of OMSs and LBSs provides more interaction force between the gas molecules and frameworks. The uptake capacity to hydrocarbons increase with the increasing of the gas polarizability ($CH_4 = 25 \times 10^{-25}$, $C_2H_6 = 44 \times 10^{-25}$, and $C_3H_8 = 63 \times 10^{-25}$ cm^3). The lowest value of Q_{st} for CH_4, which is in comparison with that of C_2H_6 and C_3H_8, indicates that the interaction between CH_4 and the adsorbent is weakest.

With regard to the application of CO_2 adsorption, the high uptake is an essential factor. Besides, the selectivity is another necessary determinant for the adsorbent since CO_2 always mixed with other gases in practical condition. Because the kinetic diameters of CO_2 and N_2 are too similar to separate, it is crucial to construct porous MOFs materials with high CO_2/N_2 selectivity. We calculated the selective separation properties of CO_2/N_2 for **JLU-Liu46** and **JLU-Liu47**. The selectivities of CO_2/N_2 (50 and 50%; 15 and 85%; and 10 and 90%) are 39, 42, and 31 for **JLU-Liu46** (Figure 6a,b) and 42, 45, and 36 for **JLU-Liu47** (Figure 6c,d), respectively. The CO_2/N_2 selectivities of **JLU-Liu46** and **JLU-Liu47** are higher than those of BUT-11(31.5),[51] BUT-10 (18.1),[51] UiO-67 (9.4),[51] NU-1000 (9),[52] and NbO-Pd-1 (33.5).[53]

The gas molecule selectivity of porous materials determines the performance of industrial fixed bed adsorbents. For a proper evaluation of the separation potential of **JLU-Liu46** and **JLU-Liu47**, we test the performances of transient breakthrough using simulation methodology.[54,55] The following parameter values were used: length of packed bed, L = 0.3 m; voidage of packed bed, ε = 0.4; and superficial gas velocity at inlet, u = 0.04 m/s.[56,57] We investigate the results of breakthrough of equimolar 4-component $CH_4/CO_2/C_2H_6/C_3H_8$ mixture in a fixed bed packed with **JLU-Liu46** and **JLU-Liu47** operated at pressure of 100 kPa and 298 K (Figure 7). The simulation results are represented in terms of a dimensionless time, τ, defined by dividing the actual time, t, by the characteristic time, $L\varepsilon/u$. The y-axis stands for the dimensionless concentration of the components at outlet of the fixed bed adsorbent. As for both **JLU-Liu46** and **JLU-Liu47**, the breakthrough of C_3H_8, C_2H_6, and CO_2 occur much later than that of CH_4, which indicates the stronger binding of C_3H_8, C_2H_6, and CO_2 as compared to that of CH_4, so the selection of adsorbents should be primarily based on CO_2/CH_4, C_2H_6/CH_4, and C_3H_8/CH_4 separation performance. Although both **JLU-Liu46** and **JLU-Liu47** have separation performance, there are definite

DOI: 10.1021/acsami.7b10795
ACS Appl. Mater. Interfaces 2017, 9, 32820−32828

distinctions in occur time of adsorbate. Therefore, combining the theoretical IAST and breakthrough simulation verified that **JLU-Liu46** and **JLU-Liu47** are promising platforms for selective adsorption and separation of C_3H_8 from the mixture of $CO_2/CH_4/C_2H_6/C_3H_8$ hydrocarbons.

Grand Canonical Monte Carlo Simulation. The density distribution of center-of-mass of CO_2 molecules in **JLU-Liu46** and **JLU-Liu47** structures were simulated by Grand Canonical Monte Carlo (GCMC) method at 298 K and 1 bar.[58] As shown in Figure 8, it reveals that CO_2 molecules in **JLU-Liu46** and **JLU-Liu47** mainly adhere to the cages, which may have strong overlapping potentials. As for the whole structure, the CO_2 molecules are apt to locate in both the open Cu metal sites and −NHCONH− groups (Figure S17). Moreover, the density of CO_2 molecules in **JLU-Liu47** (Figure 8b) is apparently higher than that in **JLU-Liu46** (Figure 8a). These results verify that the design and construction of MOFs frameworks by using polyhedron cages with more OMSs and LBSs sites would significantly enhance the CO_2 adsorption.

CONCLUSIONS

Two analogous PMOFs (**JLU-Liu46** and **JLU-Liu47**) have been designed and synthesized by utilizing the SBBs strategy. **JLU-Liu47** exhibits higher surface area and pore volume than does **JLU-Liu46** via altering the axial ligand. Benefiting from the introducing of classical Cu-paddlewheel and urea group, which provide high density of OMSs and LBSs, the two PMOFs approach high performance for CO_2 capture. Meanwhile, both of the two PMOFs materials display prominent adsorption selectivity for CO_2/CH_4 and C_3H_8/CH_4. We also point out that the synthesis strategy adopted in this work is expected to be broadly employed in the fields of constructing MOFs materials with significant CO_2 capture and gas selectivity performance for the efficient and practical applications.

ASSOCIATED CONTENT

Supporting Information

The Supporting Information is available free of charge on the ACS Publications website at DOI: 10.1021/acsami.7b10795.

PXRD, TGA, additional structural figures, and gas sorption data (PDF)

Crystallographic data for **JLU-Liu46** (CIF)

Crystallographic data for **JLU-Liu47** (CIF)

AUTHOR INFORMATION

Corresponding Author

*E-mail: yunling@jlu.edu.cn.

ORCID

Guanghua Li: 0000-0003-3029-8920

Yunling Liu: 0000-0001-5040-6816

Notes

The authors declare no competing financial interest.

ACKNOWLEDGMENTS

This work was supported by the National Natural Science Foundation of China (Nos. 21373095 and 21621001) and the 111 Project (B17020).

REFERENCES

(1) Shekhah, O.; Belmabkhout, Y.; Chen, Z.; Guillerm, V.; Cairns, A.; Adil, K.; Eddaoudi, M. Made-to-order Metal-organic Frameworks for Trace Carbon Dioxide Removal and Air Capture. *Nat. Commun.* **2014**, *5*, 4288.

(2) McDonald, T. M.; Mason, J. A.; Kong, X.; Bloch, E. D.; Gygi, D.; Dani, A.; Crocellà, V.; Giordanino, F.; Odoh, S. O.; Drisdell, W. S.; Vlaisavljevich, B.; Dzubak, A. L.; Poloni, R.; Schnell, S. K.; Planas, N.; Lee, K.; Pascal, T.; Wan, L. F.; Prendergast, D.; Neaton, J. B.; Smit, B.; Kortright, J. B.; Gagliardi, L.; Bordiga, S.; Reimer, J. A.; Long, J. R. Cooperative Insertion of CO_2 in Diamineappended Metal-organic Frameworks. *Nature* **2015**, *519*, 303−308.

(3) Li, J. R.; Ma, Y.; McCarthy, M. C.; Sculley, J.; Yu, J.; Jeong, H.; Balbuena, P. B.; Zhou, H. C. Carbon Dioxide Capture-related Gas Adsorption and Separation in Metal-organic Frameworks. *Coord. Chem. Rev.* **2011**, *255*, 1791−1823.

(4) Zhai, Q. G.; Bu, X. H.; Zhao, X.; Li, D. S.; Feng, P. Y. Pore Space Partition in Metal-organic Frameworks. *Acc. Chem. Res.* **2017**, *50*, 407−417.

(5) Nugent, P.; Belmabkhout, Y.; Burd, S. D.; Cairns, A. J.; Luebke, R.; Forrest, K.; Pham, T.; Ma, S.; Space, B.; Wojtas, L.; Eddaoudi, M.; Zaworotko, M. J. Porous Materials with Optimal Adsorption Thermodynamics and Kinetics for CO_2 Separation. *Nature* **2013**, *495*, 80−84.

(6) Adil, K.; Belmabkhout, Y.; Pillai, R. S.; Cadiau, A.; Bhatt, P. M.; Assen, A. H.; Maurin, G.; Eddaoudi, M. Gas/Vapour Separation Using Ultra-microporous Metal-organic Frameworks: Insights into the Structure/Separation Relationship. *Chem. Soc. Rev.* **2017**, *46*, 3402−3430.

(7) Cadiau, A.; Adil, K.; Bhatt, P. M.; Belmabkhout, Y.; Eddaoudi, M. A Metal-organic Framework-based Splitter for Separating Propylene from Propane. *Science* **2016**, *353*, 137−140.

(8) Cadiau, A.; Belmabkhout, Y.; Adil, K.; Bhatt, P. M.; Pillai, R. S.; Shkurenko, A.; Martineau-Corcos, C.; Maurin, G.; Eddaoudi, M. Hydrolytically Stable Fluorinated Metal-organic Frameworks for Energy-efficient Dehydration. *Science* **2017**, *356*, 731−735.

(9) Thoi, V. S.; Sun, Y.; Long, J. R.; Chang, C. J. Complexes of Earth-abundant Metals for Catalytic Electrochemical Hydrogen Generation under Aqueous Conditions. *Chem. Soc. Rev.* **2013**, *42*, 2388−2400.

(10) Yu, J.; Xie, L.; Li, J. R.; Ma, Y.; Seminario, J. M.; Balbuena, P. B. CO_2 Capture and Separations Using MOFs: Computational and Experimental Studies. *Chem. Rev.* **2017**, *117*, 9674.

(11) Mason, J. A.; Oktawiec, J.; Taylor, M. K.; Hudson, M. R.; Rodriguez, J.; Bachman, J. E.; Gonzalez, M. I.; Cervellino, A.; Guagliardi, A.; Brown, C. M.; Llewellyn, P. L.; Masciocchi, N.; Long, J. R. Methane Storage in Flexible Metal;-organic Frameworks with Intrinsic Thermal Management. *Nature* **2015**, *527*, 357−361.

(12) Mason, J. A.; Veenstra, M.; Long, J. R. Evaluating Metal-organic Frameworks for Natural Gas Storage. *Chem. Sci.* **2014**, *5*, 32−51.

(13) Li, B.; Wen, H. M.; Zhou, W.; Xu, J. Q.; Chen, B. L. Porous Metal-organic Frameworks: Promising Materials for Methane Storage. *Chem.* **2016**, *1*, 557−580.

(14) Kreno, L. E.; Leong, K.; Farha, O. K.; Allendorf, M.; Van Duyne, R. P.; Hupp, J. T. Metal-organic Framework Materials as Chemical Sensors. *Chem. Rev.* **2012**, *112*, 1105−1125.

(15) Li, H.; Eddaoudi, M.; O'Keeffe, M.; Yaghi, O. M. Design and Synthesis of an Exceptionally Stable and Highly Porous Metal-organic Framework. *Nature* **1999**, *402*, 276−279.

(16) Li, J. R.; Sculley, J.; Zhou, H. C. Metal-organic Frameworks for Separations. *Chem. Rev.* **2012**, *112*, 869−932.

(17) Alezi, D.; Belmabkhout, Y.; Suyetin, M.; Bhatt, P. M.; Weselinski, Ł. J.; Solovyeva, V.; Adil, K.; Spanopoulos, I.; Trikalitis, P. N.; Emwas, A.; Eddaoudi, M. MOF Crystal Chemistry Paving the Way to Gas Storage Needs: Aluminum-Based soc-MOF for CH_4, O_2, and CO_2 Storage. *J. Am. Chem. Soc.* **2015**, *137*, 13308−13318.

(18) Guillerm, V.; Kim, D.; Eubank, J. F.; Luebke, R.; Liu, X.; Adil, K.; Lah, M. S.; Eddaoudi, M. A Supermolecular Building Approach for the Design and Construction of Metal-organic Frameworks. *Chem. Soc. Rev.* **2014**, *43*, 6141−6172.

(19) Guillerm, V.; Weseliński, Ł.; Belmabkhout, J. Y.; Cairns, A. J.; D'Elia, V.; Wojtas, Ł.; Adil, K.; Eddaoudi, M. Discovery and Introduction of A (3,18)-Connected Net as An Ideal Blueprint for

DOI: 10.1021/acsami.7b10795
ACS Appl. Mater. Interfaces 2017, 9, 32820−32828

the Design of Metal-organic Frameworks. *Nat. Chem.* **2014**, *6*, 673−680.
(20) Xue, D. X.; Belmabkhout, Y.; Shekhah, O.; Jiang, H.; Adil, K.; Cairns, A. J.; Eddaoudi, M. Tunable Rare Earth *fcu*-MOF Platform: Access to Adsorption Kinetics Driven Gas/Vapor Separations *via* Pore Size Contraction. *J. Am. Chem. Soc.* **2015**, *137*, 5034−5040.
(21) Farha, O. K.; Yazaydin, A. Ö.; Eryazici, I.; Malliakas, C. D.; Hauser, B. G.; Kanatzidis, M. G.; Nguyen, S. T.; Snurr, R. Q.; Hupp, J. T. De *novo* Synthesis of A Metal-organic Framework Material Featuring Ultrahigh Surface Area and Gas Storage Capacities. *Nat. Chem.* **2010**, *2*, 944−948.
(22) Zheng, B.; Bai, J. F.; Duan, J.; Wojtas, L.; Zaworotko, M. J. Enhanced CO_2 Binding Affinity of A High-uptake *rht*-Type Metal-organic Framework Decorated with Acylamide Groups. *J. Am. Chem. Soc.* **2011**, *133*, 748−751.
(23) Yuan, D.; Zhao, D.; Sun, D.; Zhou, H. C. An Isoreticular Series of Metal-organic Frameworks with Dendritic Hexacarboxylate Ligands and Exceptionally High Gas-uptake Capacity. *Angew. Chem., Int. Ed.* **2010**, *49*, 5357−5361.
(24) Zhang, Z.; Li, Z.; Li, J. Computational Study of Adsorption and Separation of CO_2, CH_4, and N_2 by an *rht*-Type Metal-organic Framework. *Langmuir* **2012**, *28*, 12122−12133.
(25) Wang, X. S.; Ma, S.; Sun, D.; Parkin, S.; Zhou, H. C. A Mesoporous Metal-organic Framework with Permanent Porosity. *J. Am. Chem. Soc.* **2006**, *128*, 16474−16475.
(26) Zheng, B.; Wang, H.; Wang, Z.; Ozaki, N.; Hang, C.; Luo, X.; Huang, L.; Zeng, W.; Yang, M.; Duan, J. A Highly Porous *rht*-type Acylamide-functionalized Metal-organic Framework Exhibiting Large CO_2 Uptake Capabilities. *Chem. Commun.* **2016**, *52*, 12988−12991.
(27) Chen, B.; Ockwig, N. W.; Millward, A. R.; Contreras, D. S.; Yaghi, O. M. High H_2 Adsorption in A Microporous Metal-organic Framework with Open Metal Sites. *Angew. Chem., Int. Ed.* **2005**, *44*, 4745−4749.
(28) Eddaoudi, M.; Kim, J.; O'Keeffe, M.; Yaghi, O. M. $Cu_2[o\text{-}Br\text{-}C_6H_3(CO_2)_2]_2(H_2O)_2\ (DMF)_8(H_2O)_2$: A Framework Deliberately Designed to Have the NbO Structure Type. *J. Am. Chem. Soc.* **2002**, *124*, 376−377.
(29) Wen, H. M.; Li, B.; Yuan, D.; Wang, H.; Yildirim, T.; Zhou, W.; Chen, B. A Porous Metal-organic Framework with An Elongated Anthracene Derivative Exhibiting A High Working Capacity for the Storage of Methane. *J. Mater. Chem. A* **2014**, *2*, 11516−11522.
(30) Sun, D.; Ma, S.; Simmons, J. M.; Li, J. R.; Yuan, D.; Zhou, H. C. An Unusual Case of Symmetry-preserving Isomerism. *Chem. Commun.* **2010**, *46*, 1329−1331.
(31) Lin, X.; Telepeni, I.; Blake, A. J.; Dailly, A.; Brown, C. M.; Simmons, J. M.; Zoppi, M.; Walker, G. S.; Thomas, K. M.; Mays, T. J.; Hubberstey, P.; Champness, N. R.; Schröder, M. High Capacity Hydrogen Adsorption in Cu(II) Tetracarboxylate Framework Materials: The Role of Pore Size, Ligand Functionalization and Exposed Metal Sites. *J. Am. Chem. Soc.* **2009**, *131*, 2159−2171.
(32) Kennedy, R. D.; Krungleviciute, V.; Clingerman, D. J.; Mondloch, J. E.; Peng, Y.; Wilmer, C. E.; Sarjeant, A. A.; Snurr, R. Q.; Hupp, J. T.; Yildirim, T.; Farha, O. K.; Mirkin, C. A. Carborane-Based Metal-organic Framework with High Methane and Hydrogen Storage Capacities. *Chem. Mater.* **2013**, *25*, 3539−3543.
(33) Liu, B.; Yao, S.; Shi, C.; Li, G.; Huo, Q. S.; Liu, Y. L. Significant Enhancement of Gas Uptake Capacity and Selectivity *via* the Judicious Increase of Open Metal Sites and Lewis Basic Sites within Two Polyhedron-based Metal-organic Frameworks. *Chem. Commun.* **2016**, *52*, 3223−3226.
(34) Roberts, J. M.; Fini, B. M.; Sarjeant, A. A.; Farha, O. K.; Hupp, J. T.; Scheidt, K. A. Urea Metal-organic Frameworks as Effective and Size-Selective Hydrogen-Bond Catalysts. *J. Am. Chem. Soc.* **2012**, *134*, 3334−3337.
(35) Liu, W.; Huang, X.; Xu, C.; Chen, C.; Yang, L.; Dou, W.; Chen, W.; Yang, H.; Liu, W. A Multi-responsive Regenerable Europium-organic Framework Luminescent Sensor for Fe^{3+}, Cr^{VI} Anions, and Picric Acid. *Chem. - Eur. J.* **2016**, *22*, 18769−18776.
(36) Sheldrick, G. M. *SHELXTL-NT*, version 5.1; Bruker AXS Inc., Madison, WI, 1997.
(37) Blatov, V. A.; Shevchenko, A. P.; Proserpio, D. M. Applied Topological Analysis of Crystal Structures with the Program Package ToposPro. *Cryst. Growth Des.* **2014**, *14*, 3576−3586.
(38) Adhikari, A. K.; Lin, K.-S. Synthesis, Fine Structural Characterization, and CO_2 Adsorption Capacity of Metal Organic Frameworks-74. *J. Nanosci. Nanotechnol.* **2014**, *14*, 2709−2717.
(39) Guo, H.; Zhu, G. S.; Hewitt, I. J.; Qiu, S. L. Twin Copper Source" Growth of Metal-organic Framework Membrane: $Cu_3(BTC)_2$ with High Permeability and Selectivity for Recycling H_2. *J. Am. Chem. Soc.* **2009**, *131*, 1646−1647.
(40) Zhao, D.; Timmons, D. J.; Yuan, D.; Zhou, H. C. Tuning the Topology and Functionality of Metal-organic Frameworks by Ligand Design. *Acc. Chem. Res.* **2011**, *44*, 123−133.
(41) Park, J.; Li, J. R.; Chen, Y. P.; Yu, J.; Yakovenko, A. A.; Wang, Z. U.; Sun, L. B.; Balbuena, P. B.; Zhou, H. C. A Versatile Metal-organic Framework for Carbon Dioxide Capture and Cooperative Catalysis. *Chem. Commun.* **2012**, *48*, 9995−9997.
(42) Alsmail, N. H.; Suyetin, M.; Yan, Y.; Cabot, R.; Krap, C. P.; Lü, J.; Easun, T. L.; Bichoutskaia, E.; Lewis, W.; Blake, A. J.; Schröder, M. Analysis of High and Selective Uptake of CO_2 in An Oxamide-containing $\{Cu_2(OOCR)_4\}$ Based Metal-organic Framework. *Chem. - Eur. J.* **2014**, *20*, 7317−7324.
(43) Yan, Y.; Suyetin, M. L.; Bichoutskaia, E.; Blake, A. J.; Allan, D. R.; Barnett, S. A.; Schröder, M. Modulating the Packing of $[Cu_{24}(isophthalate)_{24}]$ Cuboctahedra in A Triazole-containing Metal-organic Polyhedral Framework. *Chem. Sci.* **2013**, *4*, 1731−1736.
(44) Venna, S. R.; Carreon, M. A. Highly Permeable Zeolite Imidazolate Framework-8 Membranes for CO_2/CH_4 Separation. *J. Am. Chem. Soc.* **2010**, *132*, 76−78.
(45) Wang, H.; Zeng, X.; Cao, D. A DIH-based Equation for Separation of CO_2-CH_4 in Metal-organic Frameworks and Covalent-organic Materials. *J. Mater. Chem. A* **2014**, *2*, 11341−11348.
(46) Chen, C. X.; Zheng, S. P.; Wei, Z. W.; Cao, C. C.; Wang, H. P.; Wang, D.; Jiang, J. J.; Fenske, D.; Su, C. Y. A Robust Metal-organic Framework Combining Open Metal Sites and Polar Groups for Methane Purification and CO_2/Fluorocarbon Capture. *Chem. - Eur. J.* **2017**, *23*, 4060−4064.
(47) Huang, Y.; Lin, Z.; Fu, H.; Wang, F.; Shen, M.; Wang, X.; Cao, R. Porous Anionic Indium-organic Framework with Enhanced Gas and Vapor Adsorption and Separation Ability. *ChemSusChem* **2014**, *7*, 2647−2653.
(48) He, Y.; Zhang, Z.; Xiang, S.; Fronczek, F. R.; Krishna, R.; Chen, B. L. A Robust Doubly Interpenetrated Metal-organic Framework Constructed from A Novel Aromatic Tricarboxylate for Highly Selective Separation of Small Hydrocarbons. *Chem. Commun.* **2012**, *48*, 6493−6495.
(49) He, Y. P.; Tan, Y. X.; Zhang, J. Tuning A Layer to a Pillared-layer Metal-organic Framework for Adsorption and Separation of Light Hydrocarbons. *Chem. Commun.* **2013**, *49*, 11323−11325.
(50) Chen, Z.; Adil, K.; Weselinski, Ł. J.; Belmabkhout, Y.; Eddaoudi, M. A Supermolecular Building Layer Approach for Gas Separation and Storage Applications: the *eea* and *rtl* MOF Platforms for CO_2 Capture and Hydrocarbon Separation. *J. Mater. Chem. A* **2015**, *3*, 6276−6281.
(51) Wang, B.; Huang, H.; Lv, X. L.; Xie, Y.; Li, M.; Li, J. R. Tuning CO_2 Selective Adsorption Over N_2 and CH_4 in UiO-67 Analogues Through Ligand Functionalization. *Inorg. Chem.* **2014**, *53*, 9254−9259.
(52) Deria, P.; Li, S.; Zhang, H.; Snurr, R. Q.; Hupp, J. T.; Farha, O. K. A MOF Platform for Incorporation of Complementary Organic Motifs for CO_2 Binding. *Chem. Commun.* **2015**, *51*, 12478−12481.
(53) Spanopoulos, I.; Bratsos, I.; Tampaxis, C.; Vourloumis, D.; Klontzas, E.; Froudakis, G. E.; Charalambopoulou, G.; Steriotis, T. A.; Trikalitis, P. N. Exceptional Gravimetric and Volumetric CO_2 Uptake in a Palladated NbO-type MOF Utilizing Cooperative Acidic and Basic, Metal-CO_2 Interactions. *Chem. Commun.* **2016**, *52*, 10559−10562.
(54) Bloch, E. D.; Queen, W. L.; Krishna, R.; Zadrozny, J. M.; Brown, C. M.; Long, J. R. Hydrocarbon Separations in a Metal-organic

DOI: 10.1021/acsami.7b10795
ACS Appl. Mater. Interfaces 2017, 9, 32820−32828

Framework with Open Iron(II) Coordination Sites. *Science* **2012**, *335*, 1606−1610.
(55) Herm, Z. R.; Wiers, B. M.; Mason, J. A.; Van Baten, J. M.; Hudson, M. R.; Zajdel, P.; Brown, C. M.; Masciocchi, N.; Krishna, R.; Long, J. R. Separation of Hexane Isomers in a Metal-organic Framework with Triangular Channels. *Science* **2013**, *340*, 960−964.
(56) Krishna, R. Methodologies for Evaluation of Metal-organic Frameworks in Separation Applications. *RSC Adv.* **2015**, *5*, 52269−52295.
(57) Krishna, R. The Maxwell-stefan Description of Mixture Diffusion in Nanoporous Crystalline Materials. *Microporous Mesoporous Mater.* **2014**, *185*, 30−50.
(58) Rappé, A. K.; Casewit, C. J.; Colwell, K. S.; Goddard, W. A.; Skiff, W. M. Application of A Universal Force Field to Main Group Compounds. *J. Am. Chem. Soc.* **1992**, *114*, 10024−10035.

DOI: 10.1021/acsami.7b10795
ACS Appl. Mater. Interfaces 2017, 9, 32820−32828

Supporting Information

Two Analogous Polyhedron-Based MOFs with High Density of Lewis Basic Sites and Open Metal Sites: Significant CO_2 Capture and Gas Selectivity Performance

Bing Liu,[a] Shuo Yao,[a] Xinyao Liu,[a] Xu Li,[b] Rajamani Krishna,[c] Guanghua Li,[a] Qisheng Huo,[a] and Yunling Liu*[a]

[a] State Key Laboratory of Inorganic Synthesis and Preparative Chemistry, College of Chemistry, Jilin University, Changchun 130012, P. R. China.
E-mail: yunling@jlu.edu.cn; Fax: +86-431-85168624; Tel: +86-431-85168614
[b] Department of Chemical and Bimolecular Engineering, National University of Singapore, 117576, Singapore.
E-mail: chelixu@nus.edu.sg.
[c] Van 't Hoff Institute for Molecular Sciences, University of Amsterdam, Science Park 904, 1098 XH Amsterdam, The Netherlands.
E-mail: r.krishna@contact.uva.cl.

Scheme for the Synthesis of H_4L:

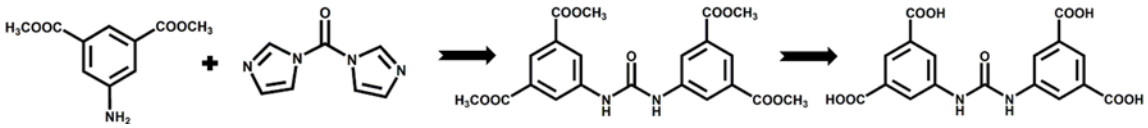

Scheme S1. Synthesis of **H_4L.**

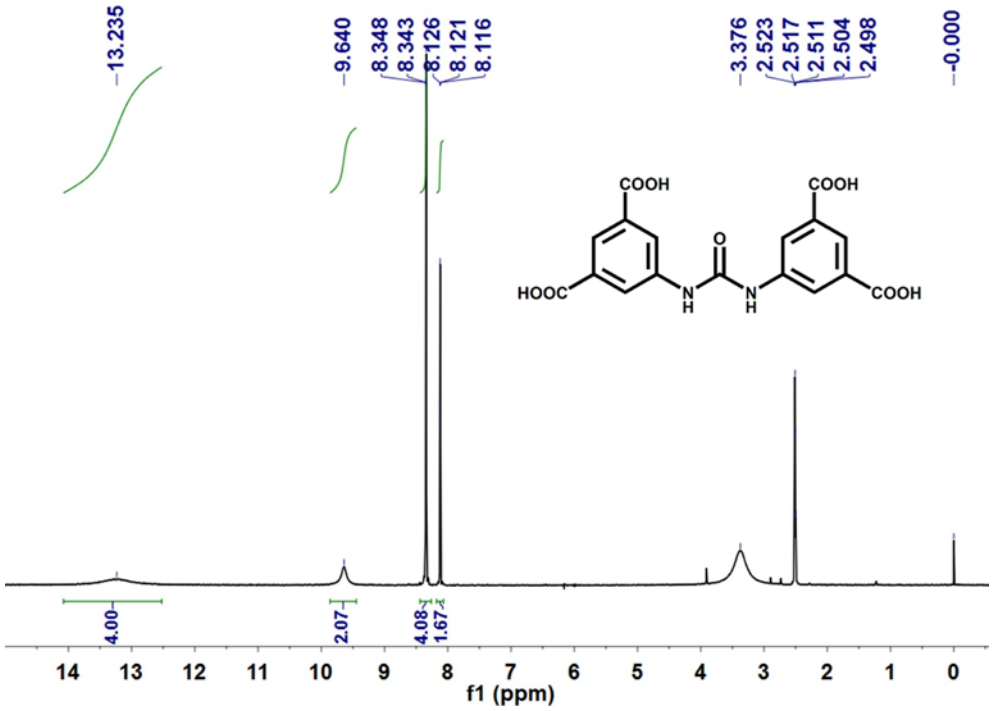

Fig. S1. H NMR spectra o**f H_4L** recorded in DMSO.

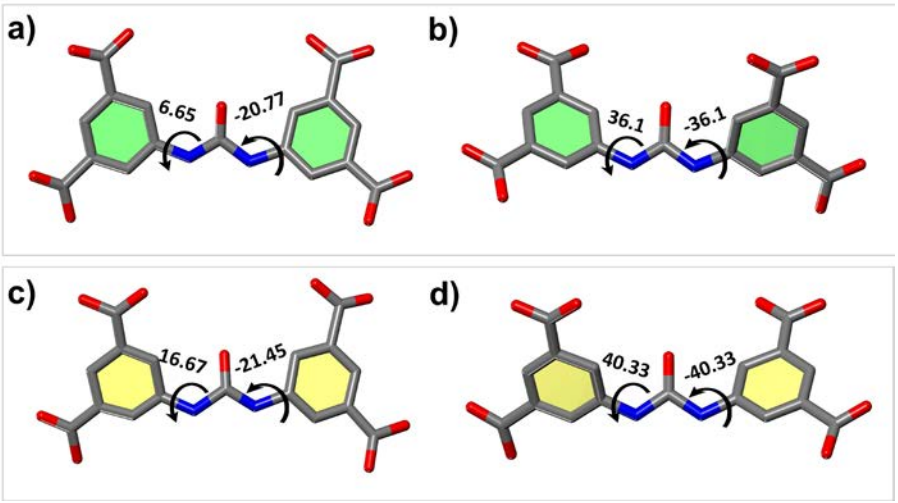

Fig. S2. 5, 5'-(carbonylbis(azanediyl)) diisophthalic acid ligands with different dihedral angles in **JLU-Liu46** (a, b) and **JLU-Liu47** (c, d).

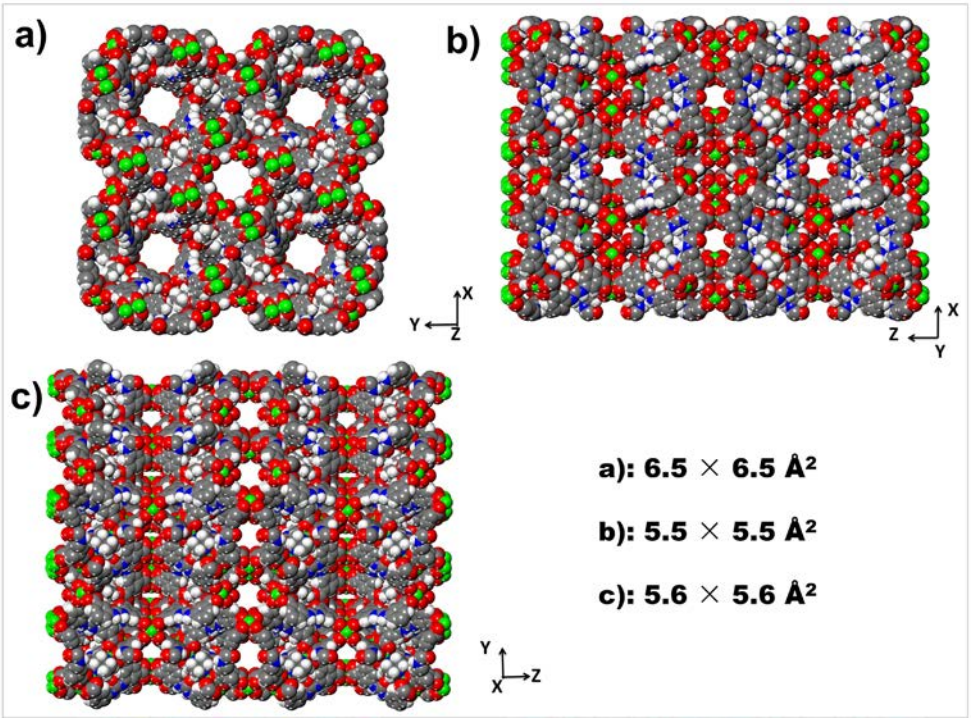

Fig. S3. Space-filling view of the structure of **JLU-Liu46** showing multiple pores in directions of (110) (a), (101) (b), (011) (c) (regardless of van der Waals radii).

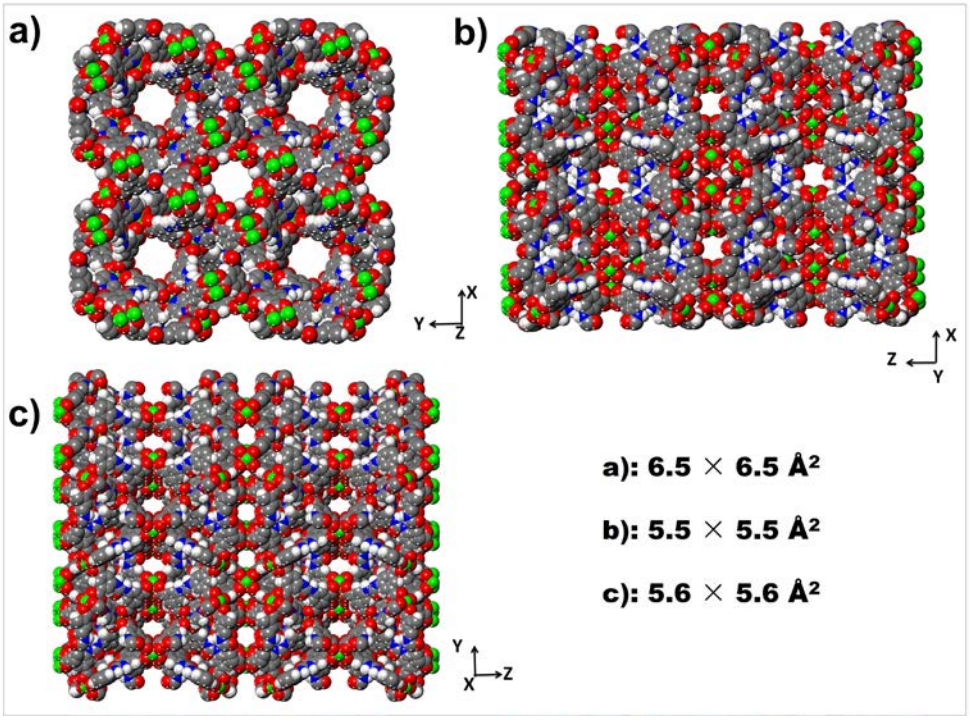

Fig. S4. Space-filling view of the structure of **JLU-Liu47** showing multiple pores in directions of (110) (a), (101) (b), (011) (c) (regardless of van der Waals radii).

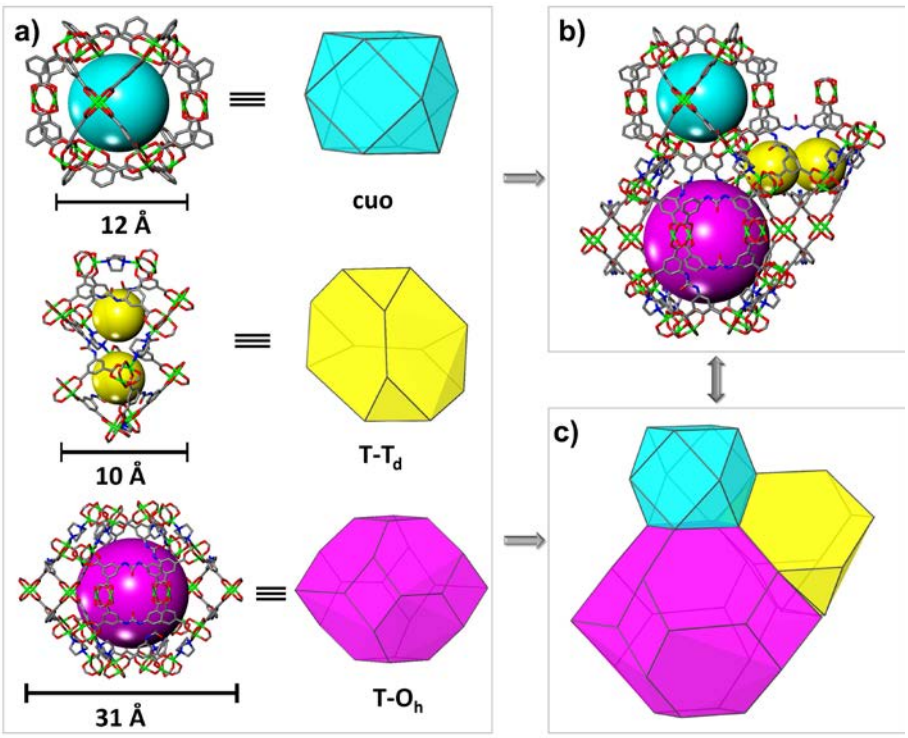

Fig. S5. View of three different cages in **JLU-Liu46** (cuboctahedron = cuo-*Oh* (bule) (a), truncated tetrahedron = T-*Td* (yellow) (b) and truncated octahedron = T-*Oh* (pink)) (c).

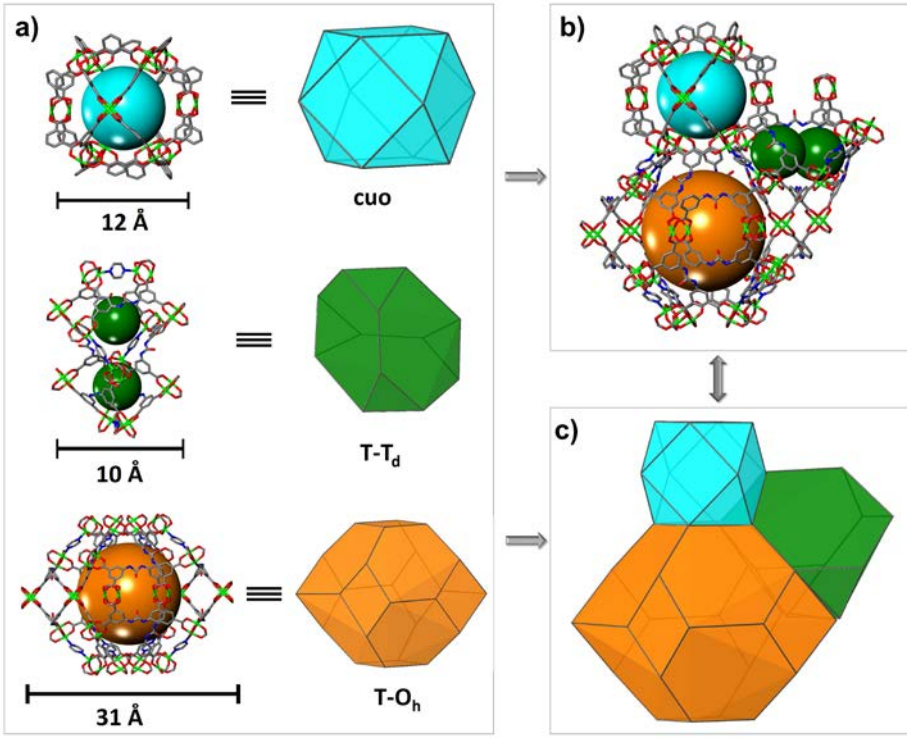

Fig. S6. View of three different cages in **JLU-Liu47** (cuboctahedron = cuo-*Oh* (bule) (a), truncated tetrahedron = T-*Td* (green) (b) and truncated octahedron = T-*Oh* (orange)) (c).

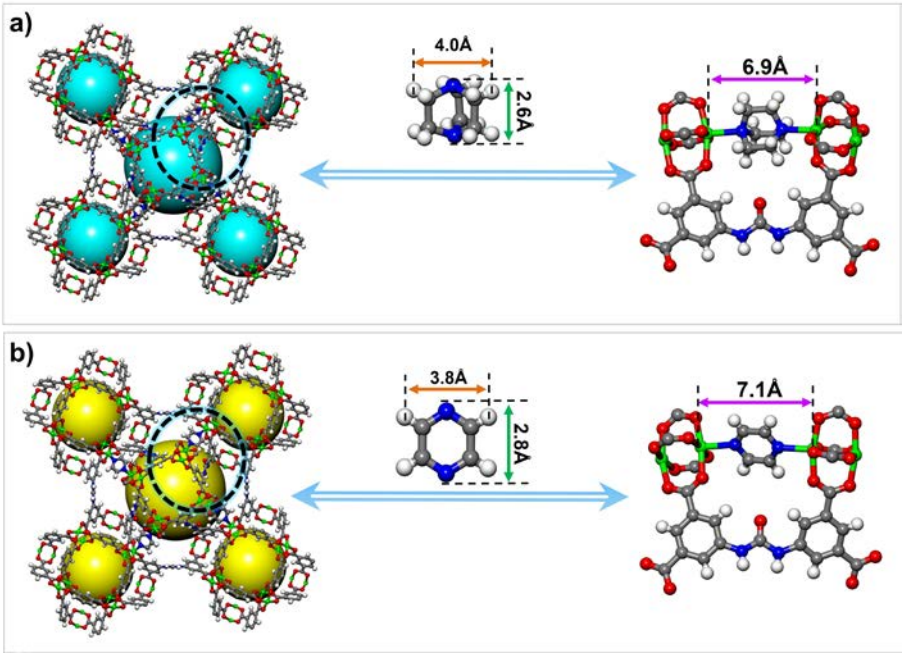

Fig. S7. The 3D framework of **JLU-Liu46** with DABCO ligand located between two paddlewheels with the precise size (a) and **JLU-Liu47** with pyrazine ligand (b).

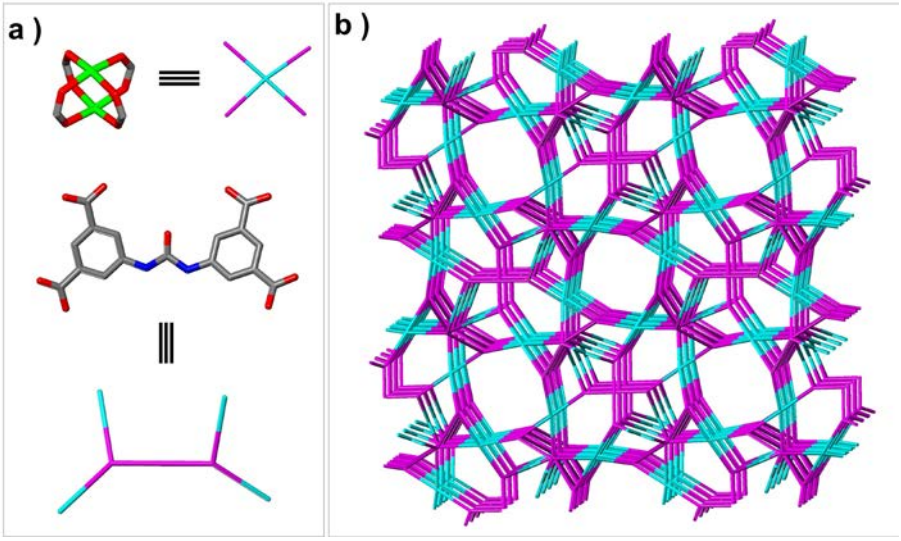

Fig. S8. Illustration of topology of **JLU-Liu46** and **JLU-Liu47**: simplification of the inorganic $Cu_2(CO_2)_4$ (4-connected node, green) and the organic **H_4L** linker (two 3-connected nodes, red) (a), leading to the new (3,4)-c net (b).

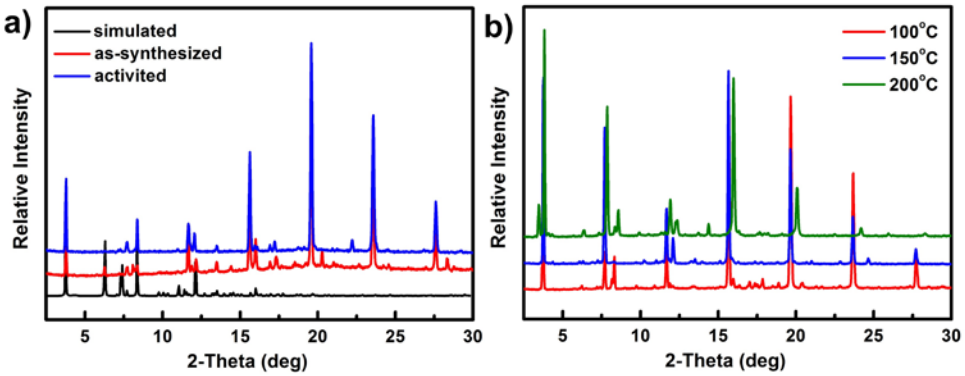

Fig. S9. (a) Simulated, as-synthesized and activated PXRD patterns for **JLU-Liu46** samples; (b) The variable-temperature PXRD patterns for **JLU-Liu46**.

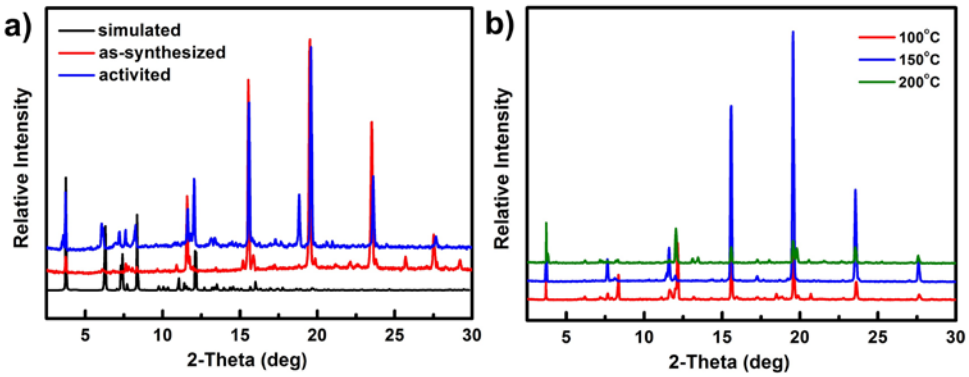

Fig. S10. (a) Simulated, as-synthesized and activated PXRD patterns for **JLU-Liu47** samples; (b) The variable-temperature PXRD patterns for **JLU-Liu47**.

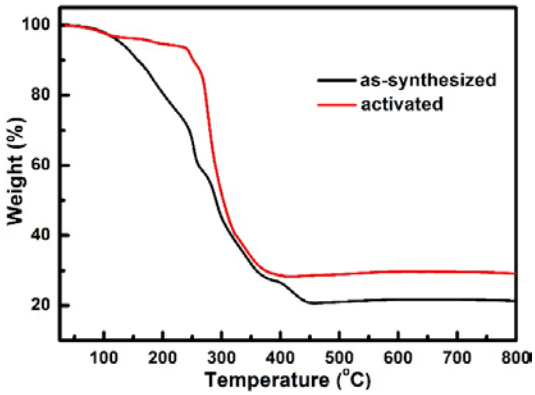

Fig. S11. TGA curves of **JLU-Liu46** for the as-synthesized and activated samples.

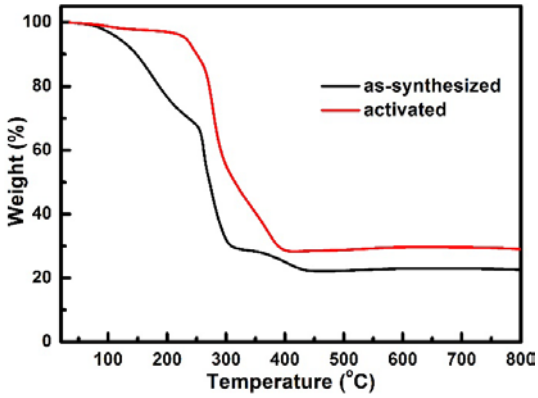

Fig. S12. TGA curves of **JLU-Liu47** for the as-synthesized and activated samples.

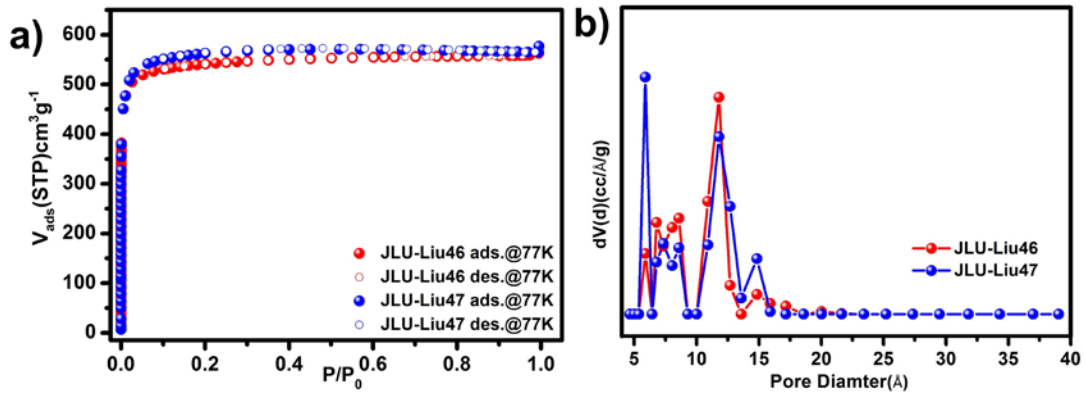

Fig. S13. (a) Nitrogen sorption isotherms on **JLU-Liu46** (red) and **JLU-Liu47** (blue) at 77 K (Adsorption: closed symbols; desorption: open symbols, respectively); (b) the pore size distribution calculated using the NLDFT method.

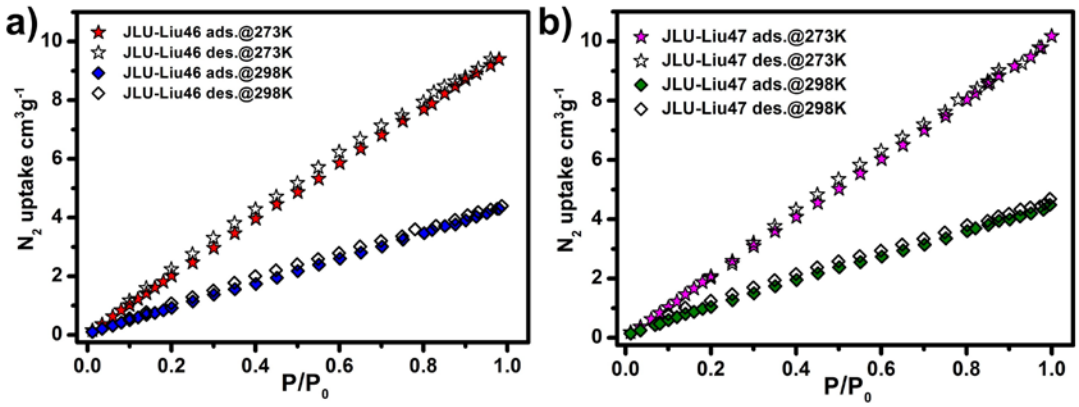

Fig. S14. The N_2 isotherm for **JLU-Liu46** (a) and **JLU-Liu47** (b) at 273 and 298 K under 1 bar.

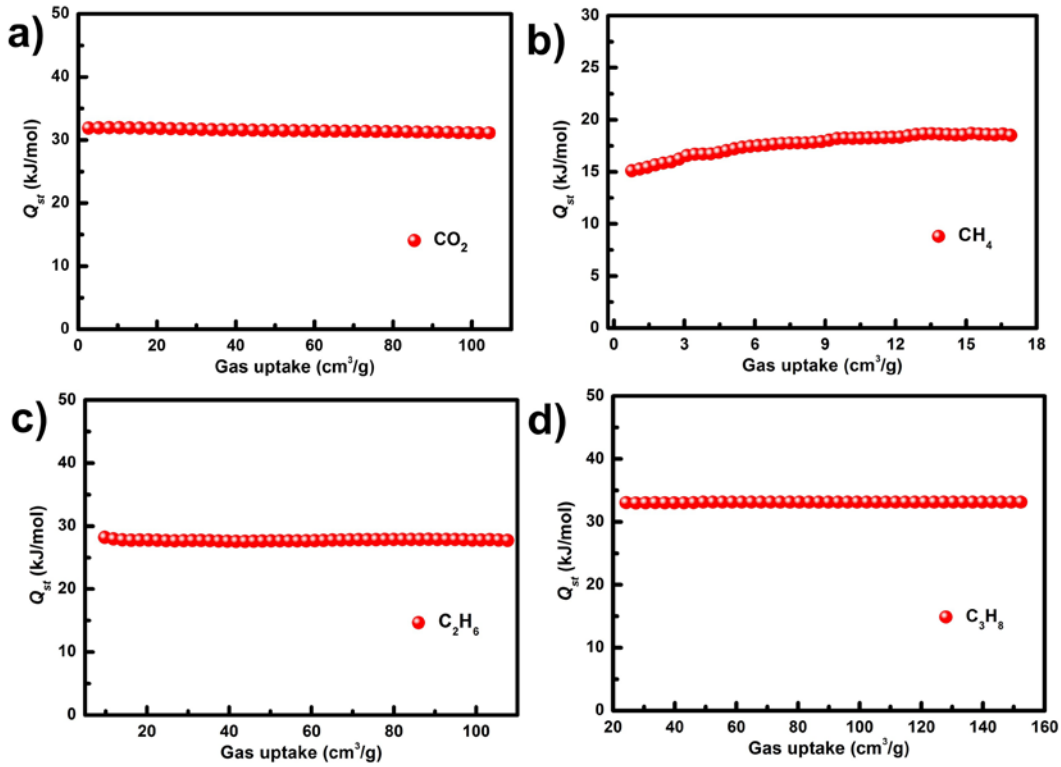

Fig. S15. Isosteric heat of CO_2 (a), CH_4 (b), C_2H_6 (c) and C_3H_8 (d) for **JLU-Liu46**.

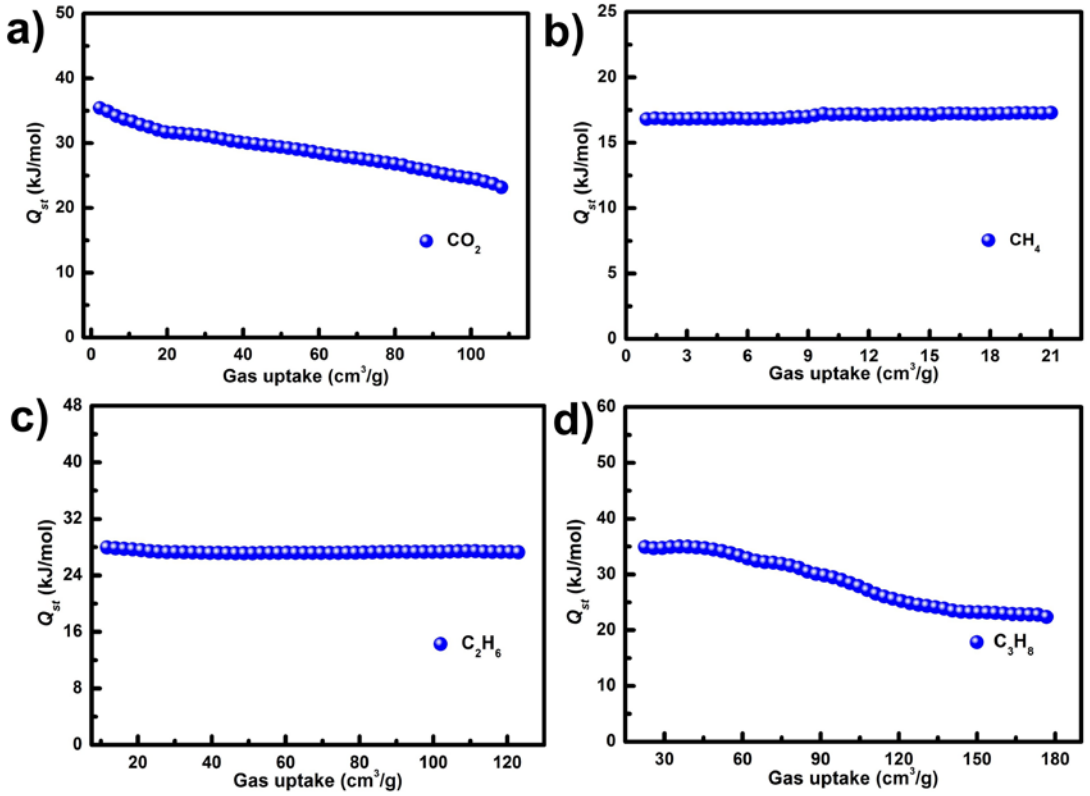

Fig. S16. Isosteric heat of CO_2 (a), CH_4 (b), C_2H_6 (c) and C_3H_8 (d) for **JLU-Liu47**.

Calculation procedures of selectivity from IAST

The measured experimental data is excess loadings (q^{ex}) of the pure components CO_2, CH_4, C_2H_6 and C_3H_8 for **JLU-Liu46** and **JLU-Liu47**, which should be converted to absolute loadings (q) firstly.

$$q = q^{ex} + \frac{pV_{pore}}{ZRT}$$

Here Z is the compressibility factor. The Peng-Robinson equation was used to estimate the value of compressibility factor to obtain the absolute loading, while the measure pore volume 0.85 $cm^3\ g^{-1}$ is also necessary.

The dual-site Langmuir-Freundlich equation is used for fitting the isotherm data at 298K.

$$q = q_{m_1} \times \frac{b_1 \times p^{1/n_1}}{1 + b_1 \times p^{1/n_1}} + q_{m_2} \times \frac{b_2 \times p^{1/n_2}}{1 + b_2 \times p^{1/n_2}}$$

Here p is the pressure of the bulk gas at equilibrium with the adsorbed phase (kPa), q is the adsorbed amount per mass of adsorbent (mol kg^{-1}), q_{m1} and q_{m2} are the saturation capacities of sites 1 and 2 (mol kg^{-1}), b_1 and b_2 are the affinity coefficients of sites 1 and 2 (1/kPa), n_1 and n_2 are the deviations from an ideal homogeneous surface.

The selectivity of preferential adsorption of component 1 over component 2 in a mixture containing 1 and 2, perhaps in the presence of other components too, can be formally defined as

$$S = \frac{q_1/q_2}{p_1/p_2}$$

q_1 and q_2 are the absolute component loadings of the adsorbed phase in the mixture. These component loadings are also termed the uptake capacities. We calculate the values of q_1 and q_2 using the Ideal Adsorbed Solution Theory (IAST) of Myers and Prausnitz.

Transient breakthrough of mixtures in fixed bed adsorbers

The performance of industrial fixed bed adsorbers is dictated by a combination of adsorption selectivity and uptake capacity. For a proper evaluation of the separation performance, we performed transient breakthrough simulations using the simulation methodology described in the literature. For the breakthrough simulations, the following parameter values were used: length of packed bed, L = 0.3 m; voidage of packed bed, ε= 0.4; superficial gas velocity at inlet, u = 0.04 m/s. The transient breakthrough simulation results are presented in terms of a *dimensionless* time, τ, defined by dividing the actual time, t, by the characteristic time, $L\varepsilon/u$.

The data on the dimensionless gas phase concentrations at the exit, vs C_i/C_{i0} dimensionless time, τ , are provided in the Excel data files.

Notation

c_i molar concentration of species *i* in gas mixture at exit of adsorber, mol m^{-3}.

c_{i0} molar concentration of species *i* in gas mixture at inlet of adsorber, mol m^{-3}.

L length of packed bed adsorber, m.

t time, s.

u superficial gas velocity in packed bed, m s^{-1}.

Grand Canonical Monte Carlo Simulations

The density distribution of CO_2 molecules in the **JLU-Liu46** and **JLU-Liu47** structures were calculated through Grand Canonical Monte Carlo (GCMC) simulation at 1 bar and 298 K. The periodic boundary conditions and Universal force field (UFF) was used. The QEq method was used to equilibrate and redistribute the overall charge of atoms of CO_2 molecules and MOF structures. The van der Waals interactions between CO_2 molecules and the MOF structures were calculated using Lennard-Jones potentials. Electrostatic interaction was evaluated through Ewald summation method. The cutoff distance was set at 18.5 Å. All the GCMC simulations were carried out using the Sorption module in Material Studio software, respectively.

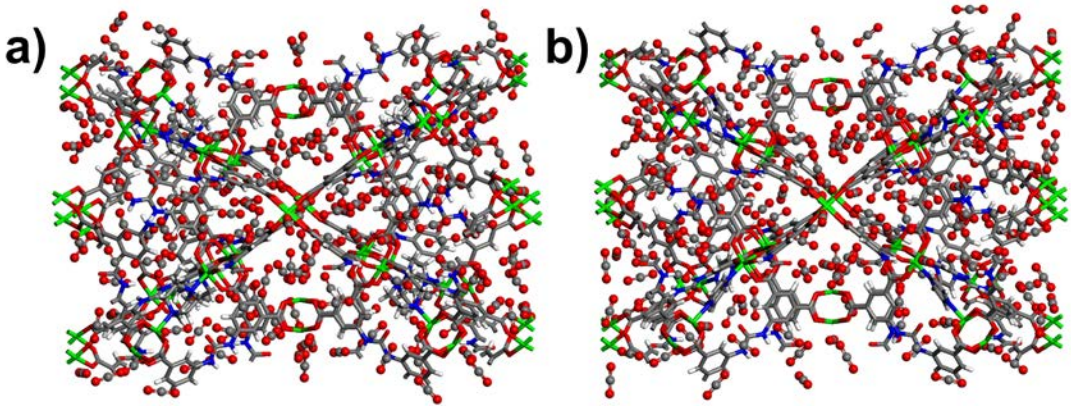

Fig. S17. Simulation snapshot for CO_2 molecules in the **JLU-Liu46** (a) and **JLU-Liu47** (b) framework.

Table S1. Crystal data and structure refinements for **JLU-Liu46** and **JLU-Liu47**.

Compound	**JLU-Liu46**	**JLU-Liu47**
Formula	$C_{72}H_{91}Cu_6N_{13}O_{42}$	$C_{70}H_{83}Cu_6N_{13}O_{42}$
Formula weight	2191.82	2159.73
Temperature (K)	293(2)	293(2)
Wavelength (Å)	0.71073	0.71073
Crystal system	Tetragonal	Tetragonal
Space group	*P4/mnc*	*P4/mnc*
a (Å)	27.199(4)	27.397(4)
b (Å)	27.199(4)	27.397(4)
c (Å)	39.140(8)	38.876(8)
α (°)	90	90
β (°)	90	90
γ (°)	90	90
V (Å^3)	28955(8)	29180(8)
Z, D_c (Mg/m^3)	8, 1.006	8, 0.983
F(000)	8992	8832
θ range (deg)	1.04-25.14	1.05-25.13
reflns collected/unique	184506 / 13133	186518 / 13240
R_{int}	0.0768	0.0788
data/restraints/params	13133/36/487	13240/24/473
GOF on F^2	1.079	1.055
R_1, wR_2 (I>2σ(I))	0.0498, 0.1572	0.0475, 0.1529
R_1, wR_2 (all data)	0.0687, 0.1668	0.0660, 0.1591

Table S2. N_2 adsorption data and structure information for **JLU-Liu46** and **JLU-Liu47**.

Compounds	SA_{BET} ($m^2\ g^{-1}$)	$SA_{Langmuir}$ ($m^2\ g^{-1}$)	Pore volume ($cm^3\ g^{-1}$) (Experimental/Theoretical)	OMSs (nm^{-3})	LBSs (nm^{-3})
JLU-Liu46	1787	2400	0.87/0.91	1.11	1.52
JLU-Liu47	1800	2493	0.90/0.93	1.09	1.50

Table S3. Summary of CO_2 uptake for top MOFs reported in the literature.

Compounds	CO_2 Ads (wt%) 273K	CO_2 Ads (wt%) 298K	Ref.
CPM-231	45.6	N. A.	1
Mg-MOF-74	44.7	29.4	2
Cu-TDPAT	44.5	25.8	3
Cu-TPBTM	42.3	23.3	4
JLU-Liu21	41.2	23.2	5
CPM-200Fe/Mg	40.7	24.9	6
NJU-Bai21	40.4	22.6	7
[Cu(Me-4py-trz-ia)]	40.5	26.8	8
NOTT-125	40.0	18.19	9
Nbo-pt-1	39.7	19.7	10
LCu'	39.0	19.3	11
SUN-5	38.5	N. A.	12
JLU-Liu47	37.7	21.2	**This work**
JLU-Liu46	36.3	20.4	**This work**
JLU-Liu20	31.8	17.3	5
PCN-88	31.4	18.4	13
rht-MOF-7	28.7	19.3	14
SIFXIX-2-Cu-i	28.6	23.8	15

N.A.: Not Available. The article do not list the data.

Table S4. Pore characteristics and CO_2 adsorption data of selected MOFs based on tetracarboxylate ligand (at 1 bar).

Compounds	Surface area ($m^2\ g^{-1}$)	CO_2 uptake (RT, wt%) 273K	298K	LBS (nm^{-1})	OMS (nm^{-1})	Ref.
Cu-MOF-1[a]	1539	46.7	21.8	2.97	0	16
NOTT-125[b]	2471	40.0	18.19	1.07	1.19	9
JLU-Liu47[c]	1800	37.7	21.2	1.09	1.50	**This work**
JLU-Liu46[c]	1787	36.3	20.4	1.11	1.52	**This work**
HNUST-1[d]	1400	30.7	18.24	0.75	0.75	17
NJU-Bai 17[e]	2423	**N.A.**	**N.A.**	1.71	0.85	18
Cu(dbda)[f]	1516	**N.A.**	**N.A.**	1.36	1.36	19
NU-601[c]	**N.A.**	**N.A.**	**N.A.**	1.19	1.19	20
$Eu_4[L]_3$[c]	**N.A.**	10.98	**N.A.**	1.17	0.78	21

a)-f) Ligands are corresponding with the above compounds. **N.A.**: Not Available. The article does not list the data.

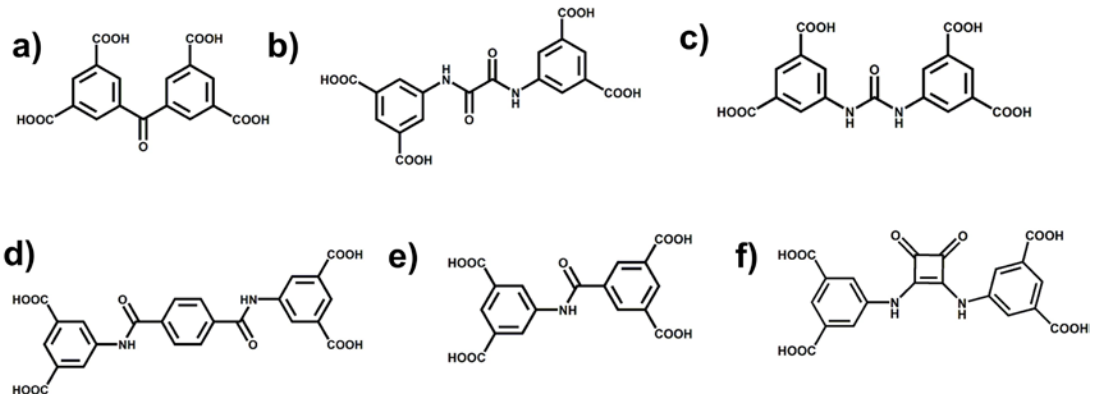

Table S5. CO_2 uptake in selected Cu-MOFs at 0.15 bar.

Compounds	CO_2 uptake (wt%)	Temperture (K)	Ref.
mmen-Cu-BTTri	9.5	298	22
SNU-5	8.1	298	23
Cu-TDPAT	7.5	298	3
CuTATB-60	5.8	298	24
NOTT-140	5.7	298	25
PMOF-3	5.3	298	26
JLU-Liu47	4.3	298	**This work**
Cu-TPBTM	4.2	298	4
NJU-Bai0	4.0	298	27
HKUST-1	3.8	298	28
JLU-Liu46	2.9	298	**This work**
SNU-50	2.9	298	29
SNU-21S	2.25	298	30
NU-100	2.16	298	31

References

1 Zhai, Q. G.; Bu, X. H.; Zhao, X.; Li, D. S.; Feng Y. P. Pore Space Partition in Metal−organic Frameworks. *Acc. Chem. Res*. **2017**, *50*, 407-417.

2. Yang, D.; Cho, H.; Kim, J.; Yang, S.; Ahn, W. CO_2 Capture and Conversion Using Mg-MOF-74 Prepared by A Sonochemical Method. *Energy Environ. Sci.,* **2012**, *5*, 6465-6473.

3. Li, B. Y.; Zhang, Z. J.; Li, Y.; Yao, K. X.; Zhu, Y. H.; Deng, Z. Y.; Yang, F.; Zhou, X. J.; Li, G. H.; Wu, H. H.; Nijem, N.; Chabal, Y. J.; Shi, Z.; Feng, S. H.; Li, J. Enhanced Binding Affinity, Remarkable Selectivity and High Capacity of CO_2 by Dual Functionalization of A *rht*-type Metal-Organic Framework. *Angew. Chem. Int. Ed.* **2012**, *51*, 1412-1415.

4 Zheng, B.; Bai, J.; Duan, J.;Wojtas, L.; Zaworotko, M. J. Enhanced, CO_2 Binding Affinity of a High-uptake *rht*-type Metal-Organic Framework Decorated with Acylamide Groups. *J. Am. Chem. Soc*. **2011**, *133*, 748-751.

5 Liu, B.; Yao, S.; Shi, C.; Li, G.; Huo, Q.; Liu, Y. L. Significant Enhancement of Gas Uptake Capacity and Selectivity *via* the Judicious Increase of Open Metal Sites and Lewis Basic Sites within Two Polyhedron Based Metal-Organic Frameworks. *Chem. Commun.* **2016**, *52*, 3223-3226.

6 Zhai, Q. G.; Bu, X.; Mao, C.; Zhao, X.; Feng, P. Systematic and Dramatic Tuning on Gas Sorption Performance in Heterometallic Metalorganic Frameworks. *J. Am. Chem. Soc.* **2016**, *138*, 2524-2527.

7 Lu, Z.; Bai, J.; Hang, C.; Meng, F.; Liu, W.; Pan, Y.; You, X. The Utilization of Amide Groups to Expand and Functionalize Metal-Organic Frameworks Simultaneously. *Chem. Eur. J.* **2016**, *22*, 6277-6285.

8 Lassig, D.; Lincke, J.; Moellmer, J.; Reichenbach, C.; Moeller, A.; Glaser, R.; Kalies, G.; Cychosz, K. A.; Thommes, M.; Staudt, R.; Krautscheid, H. A Microporous Copper Metal-Organic Framework with High H_2 and CO_2 Adsorption Capacity at Ambient Pressure. *Angew. Chem. Int. Ed.* **2011**, *50*, 10344-10348.

9 Alsmail, N. H.; Suyetin, M.; Yan, Y.; Cabot, R.; Krap, C. P.; Lü, J.; Easun, T. L.; Bichoutskaia, E.; Lewis, W.; Blake, A. J.; Schröder, M. Analysis of High and Selective Uptake of CO_2 in an Oxamide-containing $\{Cu_2(OOCR)4\}$-based Metal-Organic Framework. *Chem. Eur. J.* **2014**, *20*, 7317-7324.

10 Spanopoulos, I.; Bratsos, I.; Tampaxis, C.; Vourloumis, D.; Klontzas, E.; Froudakis, G. E.; Charalambopoulou, G.; Steriotis, T. A.; Trikalitis, P. N.

Exceptional Gravimetric and Volumetric CO_2 Uptake in A Palladated NbO-type MOF Utilizing Cooperative Acidic and Basic, Metal-CO_2 Interactions. *Chem. Commun.* **2016**, *52*, 10559-10562.

11 De, D.; Pal, T. K.; Neogi, S.; Senthilkumar, S.; Das, D.; Gupta, S. S.; Bharadwaj, P. K. A Versatile Cu^{II} Metal-Organic Framework Exhibiting High Gas Storage Capacity with Selectivity for CO_2: Conversion of CO_2 to Cyclic Carbonate and Other Catalytic Abilities. *Chem. Eur. J.* **2016**, *22*, 3387-3396.

12 Lee, Y. G.; Moon, H. R.; Cheon, Y. E.; Suh, M. P. Acomparison of the H_2 Sorption Capacities of Isostructural Metal-Organic Frameworks with and without Accessible Metal Sites: [{Zn_2(abtc) $(dmf)_2$}$_3$] and [{Cu_2(abtc) $(dmf)_2$}$_3$] Versus [{Cu_2(abtc)}$_3$]. *Angew. Chem. Int. Ed.* **2008**, *47*, 7741-7745.

13 Li, J. R.; Yu, J.; Lu, W.; Sun, L. B.; Sculley, J.; Balbuena, P. B.; Zhou, H. C. Porous Materials with Pre-designed Single-molecule Traps for CO_2 Selective Adsorption. *Nat. Commun*. **2013**, *4*, 1538.

14 Luebke, R.; Eubank, J. F.; Cairns, A. J.; Belmabkhout, Y.; Wojtas, L.; Eddaoudi, M. The Unique *rht*-MOF Platform, Ideal for Pinpointing the Functionalization and CO_2 Adsorption Relationship. *Chem. Commun.* **2012**, *48*, 1455-1457.

15 Nugent, P.; Belmabkhout, Y.; Burd, S. D.; Cairns, A. J.; Luebke, R.; Forrest, K.; Pham, T.; Ma, S.; Space, B.; Wojtas, L.; Eddaoudi, M.; Zaworotko, M. J. Porous Materials with Optimal Adsorption Thermodynamics and Kinetics for CO_2 Separation. *Nature* **2013**, *495*, 80-84.

16 Feng, G.; Peng, Y.; Liu, W.; Chang, F.; Dai, Y.; Huang, W. Polar Ketone-functionalized Metal−organic Framework Showing A High CO_2 Adsorption Performance. *Inorg. Chem.* **2017**, *56*, 2363-2366.

17 Zheng, B.; Liu, H.; Wang, Z.; Yu, X.; Yi, P.; Bai, J. F. Porous NbO-type Metal–organic Framework with Inserted Acylamide Groups Exhibiting Highly Selective CO_2 Capture. *Cryst. Eng. Comm.* **2013**, *15*, 3517-3520.

18 Zhang, M.; Li, B.; Li, Y.; Wang, Q.; Zhang, W.; Chen, B.; Li, S.; Pan, Y.; You, X.; Bai, J. F. Finely Tuning MOFs Towards High Performance in C_2H_2 Storage: Synthesis and Properties of A New MOF-505 Analogue With An Inserted Amide Functional Group. *Chem. Commun.* **2016**, *52*, 7241-7244.

19 Zhang, X.; Zhang, Z.; Boissonnault, J.; Cohen, S. M. Design and Synthesis of Squaramide-based MOFs as Efficient MOF-supported Hydrogen-bonding Organocatalysts. *Chem. Commun.* **2016**, *52*,

8585-8588.

20 Roberts, J. M.; Fini, B. M.; Sarjeant, A. A.; Farha, O. K.; Hupp, J. T.; Scheidt, K. A. Urea Metal-Organic Frameworks as Effective and Size-selective Hydrogen-bond Catalysts. *J. Am. Chem. Soc.* **2012**, *134*, 3334-3337.

21 Liu, W.; Huang, X.; Xu, C.; Chen, C.; Yang, L.; Dou, W.; Chen, W.; Yang, H.; Liu, W. A Multi-responsive Regenerable Europium-organic Framework Luminescent Sensor for Fe^{3+}, Cr^{VI} Anions, and Picric Acid. *Chem. Eur. J.* **2016**, *22*, 18769-18776.

22 McDonald, T. M.; D'Alessandro, D. M.; Krishna, R.; Long, J. R. Enhanced Carbon Dioxide Capture Upon Incorporation of N,N '-Dimethylethylenediamine in the Metal-Organic Framework CuBTTri. *Chem. Sci.*, **2011**, *2*, 2022-2028.

23 Lee, Y.-G.; Moon, H. R.; Cheon, Y. E.; Suh, M. P. A Comparison of the H_2 Sorption Capacities of Isostructural Metal–organic Frameworks with and without Accessible Metal Sites: $[\{Zn_2(abtc)(dmf)_2\}_3]$ and $[\{Cu_2(abtc)(dmf)_2\}_3]$ versus $[\{Cu_2(abtc)\}_3]$. *Angew. Chem. Int. Ed.*, **2008**, *47*, 7741–7745.

24 Kim, J.; Yang, S.-T.; Choi, S. B.; Sim, J.; Kim, J.; Ahn, W.-S. Control of Catenation in CuTATB-n Metal-Organic Frameworks by Sonochemical Synthesis and Its Effect on CO_2 Adsorption. *J. Mater. Chem.*, **2011**, *21*, 3070-3076.

25 Tan, C.; Yang, S.; Champness, N. R.; Lin, X.; Blake, A. J.; Lewis, W.; Schroder, M. High Capacity Gas Storage by a 4,8-connected Metal–organic Polyhedral Framework. *Chem. Commun.*, **2011**, *47*, 4487–4489.

26 Liu, X.; Park, M.; Hong, S.; Oh, M.; Yoon, J. W.; Chang, J.-S.; Lah, M. S. A Twofold Interpenetrating Porous Metal-Organic Framework with High Hydrothermal Stability: Structure and Gas Sorption Behavior. *Inorg. Chem.*, **2009**, *48*, 11507–11509.

27 Wang, Q.; Bai, J.; Lu, Z.; Pan, Y.; You, X.; Finely Tuning MOFs towards High-performance Post-combustion CO_2 Capture Materials. *Chem. Commun*., **2016**, *52*, 443-452.

28 Zhang, Z.; Zhao, Y.; Gong, Q.; Li, Z.; Li, J. MOFs for CO_2 Capture and Separation from Flue Gas Mixtures: the Effect of Multifunctional Sites on their Adsorption Capacity and Selectivity. *Chem. Commun.*, **2013**, 49, 653-661.

29 Prasad, T. K.; Hong, D. H.; Suh, M. P. High Gas Sorption and Metal-ion Exchange of Microporous Metal-Organic Frameworks with Incorporated Imide Groups. *Chem. Eur. J.*, **2010**, *16*, 14043-14050.

30 Kim, T. K.; Suh, M. P. Selective CO_2 Adsorption in a Flexible Non-interpenetrated Metal–organic Framework. *Chem. Commun.*, **2011**, *47*, 4258–4260.

31 Farha, O. K.; Yazaydın, A. Ö.; Eryazici, I.; Malliakas, C. D.; Hauser, B. G.; Kanatzidis, M. G.; Nguyen, S. T.; Snurr, R. Q.; Hupp, J. T. De *novo* Synthesis of a Metal–organic Framework Material Featuring Ultrahigh Surface Area and Gas Storage Capacities. *Nat. Chem.*, **2010**, *2*, 944–948.